DEVELOPMENT OF A TOOLBOX FOR SIMULATION OF INTEGRATED RESERVOIR-PRODUCTION SYSTEM

A Thesis

by

ZIHAO CHEN

Submitted to the Office of Graduate and Professional Studies of
Texas A&M University
in partial fulfillment of the requirements for the degree of

MASTER OF SCIENCE

Chair of Committee,	Eduardo Gildin
Committee Members,	Ibere Alves
	Zenon Medina-Cetina
Head of Department,	Jeff Spath

December 2020

Major Subject: Petroleum Engineering

ABSTRACT

The simulation of an integrated reservoir-production system is often suggested or even required to develop offshore oil fields. The pressure drop in the production system is a significant factor to consider in well placement and the selection of production strategy. The simulation of the coupled system can improve accuracy and help optimize the production strategy for higher production and financial outcomes. Methods to couple the production system with the reservoir system fall into three categories: explicit coupling, partially implicit coupling, and implicit coupling method. The implicit coupling method solves both systems in one simulator providing high stability but suffers from high computational cost. The explicit coupling method is flexible in terms of the choices of different simulators. The explicit coupling method has the least computational cost but suffers from unstable results (oscillations). In this study, the MATLAB Reservoir Simulation Toolbox (MRST) is an open-source reservoir simulator used for coupling with the surface network. A surface network modeling module and a reservoir-production system explicitly coupling module are developed to couple with MRST. A new method of obtaining average drainage area pressure for calculating the IPR (Inflow Performance Relationship) curve is developed. The new method is also evaluated on its effectiveness in reducing the instabilities. The new method is ineffective in lowering oscillations for simulations with a large size of time steps but may be useful for smaller time steps. The application of this toolbox is demonstrated with two models, a simplistic, "shoe-box" like model, and a complex model, UNISIM-I-D. UNISIM-I-D is a synthetic numerical model based on the Namorado field, an offshore field in Brazil.

ACKNOWLEDGEMENTS

I would like to acknowledge Dr. Gildin for his guidance and support throughout the course of this research, and during my time at Texas A&M. I would also like to thank my committee members, Dr. Alves and Dr. Medina-Cetina.

I would also like to acknowledge Kíldare George Ramos Gurjão and Marcelo Dall'Aqua for their generous support in this study.

Thanks also go to my friends and the department faculty and staff for making my time at Texas A&M University a great experience.

CONTRIBUTORS AND FUNDING SOURCES

Contributors

This work was supervised by a thesis committee consisting of Professor Gildin [advisor], Professor Alves [member] of the Harold Vance Department of Petroleum Engineering, and Professor Medina-Cetina [member] of the Department of Civil & Environmental Engineering.

All work for the thesis was completed independently by the student. There was no outside funding that supported this research. The student funded his own research.

NOMENCLATURE

A	Cross-section area
avg	Discrete average operator
b	Shrinkage factor
B	Formation volume factor
BHP	Bottom-hole pressure
c	Cell value
c_t	Isothermal compressibility
d	Tubing/pipe diameter
div	Discrete divergence operator
f	Friction factor
f_n	Non-Slip friction factor
f_{tf}	Two-phase friction factor
g	Gravitational Acceleration
G	Mass flux rate
grad	Discrete gradient operator
$E_i(x)$	Exponential integral function
h	Formation thickness
H_L	Liquid holdup
II	Injectivity index
IPR	Inflow Performance Relationship
J	Productivity index
K	Permeability
k_r	Relative permeability
N_{FR}	Froude number
N_{Lv}	Liquid velocity number
N_{Re}	Reynolds number
OPR	Outflow Performance Relationship
p	Pressure
p_1	Pressure at upstream of the choke

p_4	Pressure at downstream of the choke
$\bar{p}$	Average drainage pressure
p_{block}	Well block pressure
p_i	Initial pressure
p_{wf}	Wellbore flowing pressure
PI	Productivity index
q	Flow rate
r	radius
r_e	Reservoir radius
r_w	Wellbore radius
R_S	Solution gas-oil ratio
R_{gl}	Producing gas-liquid ratio
S	Skin factor
S	Saturation
t	time
T[*f*]	Face-valued pressure
upw	Phase-upwind function
v	Velocity
v_s	Superficial velocity
v[f]	Flux on face *f*
V	Volume
z	Distance in Z-Direction of Cartesian

Coordinate

Greek Letters

α	Phases = o,w,g
γ	Euler's constant
Δt	Timestep
μ	Viscosity
λ	Phase mobility
λ_L	No-slip liquid holdup

ρ	Density
ϕ	Porosity

Subscripts

b	bubble point
g	Gas
go	Gas-oil
gw	Gas-water
l	Liquid
m	Mixture
o	Oil
ow	Oil-water
res	Reservoir
sc	At standard conditions
t	Total
w	Water

TABLE OF CONTENTS

Page

LIST OF FIGURES

Page

LIST OF TABLES

Page

1. INTRODUCTION

In the oil production process, the pressure drop in the production system is a significant factor in well placement and the selection of production strategy, especially for offshore oil fields. The well deliverability is affected by the pressure drop in the production system, which is an additional constraint for wells in reservoir simulation. Therefore, it's necessary to perform a reservoir-production system coupling because the constraint from the production system usually changes during oil production. The coupling of the production system with reservoir simulation is typically required for offshore fields. Additional components complicate the production system at seafloor levels, such as manifolds that collect and combine flow from several wells. As a result of coupling surface flow with the reservoir flow, the prediction of well performance is more accurate. By further optimizing the production strategy, one could potentially achieve higher production and financial outcomes.

There are many ways to couple the production system with the reservoir system. The reservoir-production system coupling methods are typically categorized by how information is exchanged between the production simulator and reservoir simulator and fall into three categories: explicit coupling, partially implicit coupling, and implicit coupling (Hiebert et al., 2011). The explicit coupling method exchanges information between the surface modeling program and reservoir simulator at the end of each time step. In explicit coupling, the reservoir simulation is solved at fixed time steps. At the end of each time step, the reservoir simulation passes the calculated solution of each well to the surface modeling program. The coupling module assembles the well performance curve from both reservoir and production program and determines the operating points for each

well. Then, the reservoir simulator obtains these operating points for the simulation of the next time step. The partially implicit coupling method follows a procedure similar to the explicit coupling method but exchanges information at the Newton iteration level. According to Guyaguler et al. (2011), the balancing frequency of the explicit coupling method is also known as time step lagged. The balancing frequency of the partially implicit coupling method is iteratively lagged. The scheme of the explicit coupling method and the partially implicit coupling method are shown in figure 1.1. Unlike the explicit coupling and partially implicit coupling method, the implicit coupling method combined the reservoir simulation and surface modeling into one simulator. The simulator solves both reservoir equations and surface flow equations simultaneously. The implicit coupling method could avoid oscillation problems common in explicit coupling but at a high computational cost. On the contrary, the explicit coupling has a low computational cost but may experience non-physical oscillations with large time steps.

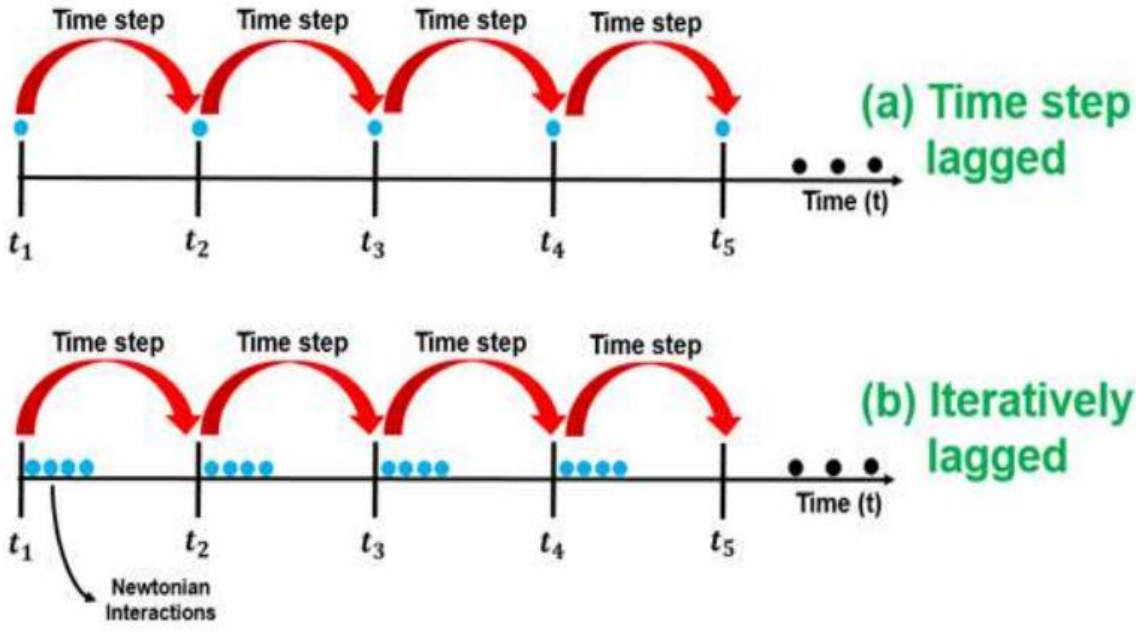

Figure 1.1 Scheme of explicit and partially implicit coupling process reprinted from (Gurjão, 2018).

In the explicit coupling process, the inflow performance curve (IPR) is constructed using the calculated solution from the reservoir simulator. The traditional IPR calculation is based on Peaceman's equation (1978), with the steady-state-radial flow assumption, where block pressure is used to estimate reservoir pressure. The instability of block pressure is considered as one of the reasons for non-physical oscillation in the explicit coupling method. Many techniques are proposed to alter the traditional IPR calculation, such as simulating two simultaneous flow tests to calculate IPR based on the drainage region (Liang and Rubin, 2013) and determining a stable pressure with the PID controller for IPR calculation (Gurjão, 2018). Also, other techniques proposed to reduce the coupling instability includes correlating block pressure with flow rate (Hohendorff Filho & Schiozer, 2016) and determining the optimum time step size using the PID controller (Redick, 2017).

In this study, a toolbox containing a surface-flow modeling module and a coupling module is developed for an open-source reservoir simulator. Using this toolbox and the reservoir simulator, a method to determine average drainage area pressure for IPR calculation is applied and evaluated in two case studies.

1.1. Motivation

The MATLAB Reservoir Simulation Toolbox (MRST) is a free and open-source reservoir simulator that contains fully implicit solvers and utilizes automatic differentiation. It is capable of rapid prototyping methods and modeling concepts. However, MRST does not have a module to model the surface network system or coupling reservoir flow with the surface network. Therefore, this work was dedicated to the development of a surface coupling module for MRST that is capable of modeling flow in

surface networking and coupling the surface flow with the subsurface flow from the reservoir simulator.

Also, after reviewing the literature on explicit coupling, it's known that non-physical oscillation for explicit coupling can be a problem that results in unstable solutions, an example of a non-physical oscillation result is shown in figure 1.2, and in work done by Hayder (2010). Previous works developed methods to reduce time step sizes with the PID controller and determine a stable pressure with the PID controller (Redick, 2017; Gurjão, 2018). Another work done by Liang and Rubin (2013) is replacing well block pressure with average drainage pressure that could be a solution to the oscillation problem. However, the work by Liang and Rubin requires running two simultaneous flow tests with a high cost of computation. A new method is proposed to obtain the drainage area pressure with a shorter flow test.

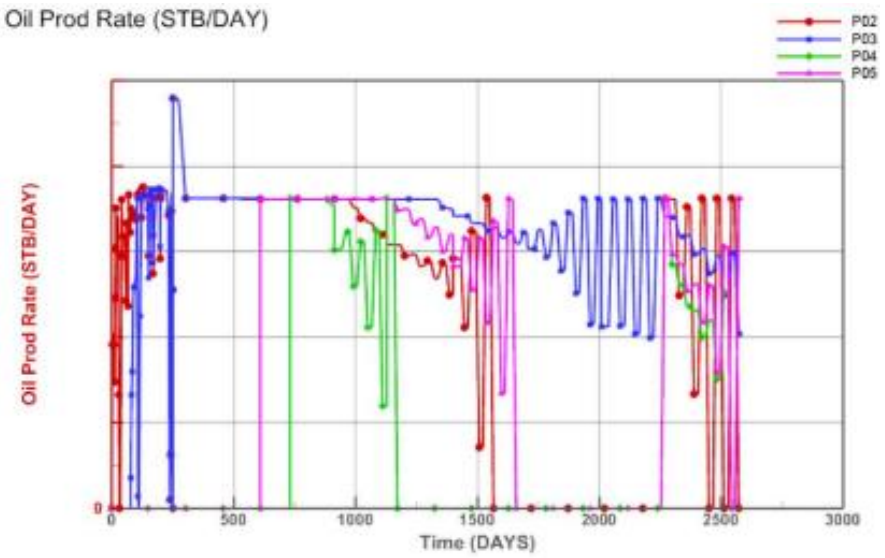

Figure 1.2 An Example of A Non-Physical Oscillation Result reprinted from (Zhang et al., 2017).

1.2. Objectives

This work has the following three objectives:

1. Development of a toolbox for the reservoir simulation platform called MRST, which is capable of simulating surface flow and coupling the surface network with the reservoir system.
2. Development of a systematic approach to calculate the drainage pressure around a well and its respective IPR curves
3. The assessment of the new IPR on two models that involve coupled surface-subsurface: (1) a simplistic shoebox-like model with flowlines and chokes, and (2) a more realistic reservoir with complex geometry and characteristics and multiple wells.
4. The analysis of potential oscillations commonly encountered in coupled problems and the assessment of new IPR calculations as a way to mitigate the oscillation.

1.3. Organization

This work is organized into seven chapters. Chapter two introduces the equations for the multiphase black-oil model and the discretization of these equations in MRST using vectorized operators. Chapter three provides the background of well representation, including the analytical solutions of the diffusivity equation and the method to construct well deliverability. Chapter four introduces the proposed method for creating IPR and OPR and obtaining the operating point. The design and workflow of the toolbox are also demonstrated. Chapters five discussed the application and results of explicit coupling for two case studies and followed by analyses of potential oscillations and assessing the new IPR calculation method. Chapter seven ends with a conclusion and suggestions for future work.

2. MULTIPHASE FLOW RESERVOIR MODELING AND SIMULATION

In reservoir simulation, the subsurface domain is represented by a geological model that is composed of the grid model with petrophysical properties. With the reservoir characterization method, the porous medium in the subsurface domain could be represented by millions of grid-blocks. However, these detailed geological grid models are rarely used for simulation because of the high computational cost. Instead, upscaled models are usually used along with mathematical flow models that describe the fluid flow (Lie, 2019). Besides, a well model is also required to connect the subsurface domain with the surface, providing an outlet for the reservoir connected to the surface network.

The reservoir simulators can be classified based on the reservoir fluid property models, including gas, black-oil, and compositional models. The compositional model is generally used for a simulation that is sensitive to compositional changes in the reservoir fluids. The black-oil model is used when the compositional changes in reservoir fluids are insignificant in the recovery process. In the black-oil model, mass transfer is considered strictly pressure-dependent, and PVT behavior of the reservoir fluid is controlled by formation volume factors and solution gas-oil ratio.

In this study, the black-oil model is used as the fluid model, and the black-oil equations are introduced later in this chapter. Besides, the MATLAB Reservoir Simulation Toolbox (MRST), which is the simulator used for this study, and its highly vectorized discrete operators are also introduced. The discretization of the black-oil partial differential equations in MRST using the discrete operators is shown at the end of this chapter.

2.1. The Black-oil Model

The black-oil model includes the flow of three fluid components, oil, gas, and water, in at most three phases. Each fluid component is contained within its phase, except that the gas component is soluble only in oil, as shown in figure 2.1. The water component is considered immiscible with the other two components, and therefore, no mass transfer between water and other phases (Ertekin et al. 2000).

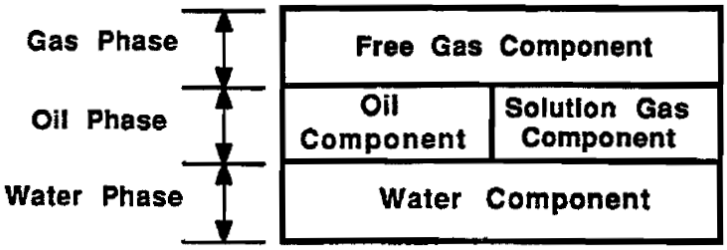

Figure 2.1 Distribution of components below the bubble point.

The dissolved gas component in the oil phase is known as solution gas, and the solubility of the gas in oil is known as the solution gas-oil ratio, defined as the ratio of the volume of gas coming out of solution to the volume of oil at standard conditions and denoted by R_s.

$$R_s = \frac{V_{g,sc}}{V_{o,sc}}. \tag{2.1}$$

Saturation is defined as the fraction of volume occupied by phase α, denoted by S_α. Bubble point pressure is defined as the pressure where natural gas begins to come out of solution and forming bubbles. Bubble point pressure could be obtained from PVT table or black-oil correlations. When reservoir pressure is above bubble point pressure, the reservoir is undersaturated where no free gas is present in the reservoir, so that

$$S_o + S_w = 1,\ R_s = 0 \ \text{ when } \ P_{res} > P_b. \tag{2.2}$$

When reservoir pressure decreased below bubble point pressure, the reservoir becomes saturated and start forming a gas phase so that

$$S_o + S_w + S_g = 1,\ R_s > 0 \ \text{ when } \ P_{res} < P_b. \tag{2.3}$$

The governing equations are introduced in the next section.

2.2. Governing Equations for Multiphase-Flow

The material-balance equation is one of the governing equations for fluid-flow modeling. The partial differential equation has three terms: accumulation, flux, and source and sink, representing the mass transfer of each component across each controlled volume. Following Lie (2019), the general form of this PDE for one component in each phase can be represented as:

$$\underbrace{\frac{\partial}{\partial t}\left(\phi \rho_\alpha S_\alpha\right)}_{\text{Accumulation}} + \underbrace{\nabla\left(\rho_\alpha \vec{v}_\alpha\right)}_{\text{Flux}} = \underbrace{\rho_\alpha q_\alpha}_{\text{Source and Sink}} . \tag{2.4}$$

The mass fraction of components l in phase α, denoted by c^l_α, is included to form the multiple-component, multiphase flow mass-balance equation,

$$\underbrace{\frac{\partial}{\partial t}\left(\phi \sum_\alpha c^l_\alpha \rho_\alpha S_\alpha\right)}_{\text{Accumulation}} + \underbrace{\nabla\left(\sum_\alpha c^l_\alpha \rho_\alpha \vec{v}_\alpha + \vec{J}^l_\alpha\right)}_{\text{Flux}} = \underbrace{\sum_\alpha c^l_\alpha \rho_\alpha q_\alpha}_{\text{Source and Sink}} . \tag{2.5}$$

Where J is diffusion and is ignored for the black-oil model, and $\alpha = o, w, g$

The formation volume factor for phase α, denoted by B_α, is defined as the ratio of the volume at reservoir condition to the volume at standard conditions. When substitute volume with density $\rho_\alpha = m_a / V_\alpha$, the formation volume factor is given by:

$$B_\alpha = \frac{V_\alpha}{V_{\alpha,sc}} = \frac{\rho_{\alpha,sc}}{\rho_\alpha}. \tag{2.6}$$

By substituting equation (2.1) and (2.6) into (2.5), the conservation equations for components oil, water and gas are provided by:

$$\frac{\partial}{\partial t}\left(\frac{\phi S_o}{B_o}\right) + \nabla\left(\frac{\vec{v}_o}{B_o}\right) = \frac{q_o}{B_o}. \tag{2.7}$$

$$\frac{\partial}{\partial t}\left(\frac{\phi S_w}{B_w}\right) + \nabla\left(\frac{\vec{v}_w}{B_w}\right) = \frac{q_w}{B_w}. \tag{2.8}$$

$$\frac{\partial}{\partial t}\left(\frac{\phi S_g}{B_g} + \frac{\phi S_o R_s}{B_o}\right) + \nabla\left(\frac{\vec{v}_g}{B_g} + \frac{\vec{v}_o R_s}{B_o}\right) = \frac{q_g}{B_g} + \frac{q_o R_s}{B_o}. \tag{2.9}$$

Another governing equation for the multiphase-flow model is Darcy's law, which is extended from the single-phase flow equation by applying the relative permeability of each phase. The Darcy's law equation for each phase is given by:

$$\vec{v}_\alpha = -\frac{K k_{r\alpha}}{\mu_\alpha}\left(\nabla p_\alpha - \rho_\alpha g \nabla z\right). \tag{2.10}$$

The front portion of Darcy's equation is also known as the mobility, and in the multiphase-phase flow, it's known as the phase mobility:

$$\lambda_\alpha = \frac{K k_{r\alpha}}{\mu_\alpha}. \tag{2.11}$$

By substituting equation (2.10) and (2.11) into equations (2.7)-(2.9), rearranging yields:

$$\frac{\partial}{\partial t}\left(\frac{\phi S_o}{B_o}\right) - \nabla\left(\frac{\lambda_o\left(\nabla p_o - \rho_o g \nabla z\right)}{B_o}\right) = \frac{q_o}{B_o}. \tag{2.12}$$

$$\frac{\partial}{\partial t}\left(\frac{\phi S_w}{B_w}\right) - \nabla\left(\frac{\lambda_w\left(\nabla p_w - \rho_w g \nabla z\right)}{B_w}\right) = \frac{q_w}{B_w}. \tag{2.13}$$

$$\frac{\partial}{\partial t}\left(\frac{\phi S_g}{B_g}+\frac{\phi S_o R_s}{B_o}\right)-\nabla\left(\frac{\lambda_g\left(\nabla p_g-\rho_g g\nabla z\right)}{B_g}+\frac{\lambda_o R_s\left(\nabla p_o-\rho_o g\nabla z\right)}{B_o}\right)=\frac{q_g}{B_g}+\frac{q_o R_s}{B_o}. \quad (2.14)$$

Besides the saturation constraint in equations (2.2) and (2.3), other relationships required for solving the partial differential equations above are capillary pressures and relative permeability as functions of saturation, which could be related as a function of phase pressure:

$$P_{cow}\left(S_w,S_o\right)=p_o-p_w, \quad (2.15)$$

$$P_{cgo}\left(S_o,S_g\right)=p_g-p_o, \quad (2.16)$$

$$P_{cgw}=P_{cgo}\left(S_o,S_g\right)-P_{cow}\left(S_w,S_o\right), \quad (2.17)$$

$$k_{rw}=\left(\hat{S}_w\right)^{n_w}k_w^0 \quad \text{and} \quad k_{ro}=\left(1-\hat{S}_w\right)^{n_o}k_o^0, \quad (2.18)$$

The equation (2.18) is also known as the Corey model, where n_w, n_o >= 1, and k_α^0 is a scaling constant. The relative permeability equation could be replaced by other relations or interpreting permeability and PVT tables.

2.3. The MATLAB Reservoir Simulation Toolbox (MRST)

The MATLAB Reservoir Simulation Toolbox (MRST) is an open-source and object-oriented simulator. Therefore, it is capable of rapid prototyping, creating new models, and demonstrating methods for reservoir simulation studies. The fundamental part of the toolbox is the MRST-AD framework, which combines the following essential functionalities (Lie et al., 2012):

- Flexible grid structure

- Highly vectorized operators
- Fully implicit solvers with automatic differentiation
- Automatic differentiation setup for physical properties.

The grid structure in MRST sacrificed some efficiency to achieve maximum flexibility to support a large variety of grid types in which non-matching faces are converted to the general format. As a result of this flexibility, the grid module supports creating not only structured grids, including regular Cartesian, rectilinear, and curvilinear grids, but also unstructured grids, including Delaunay triangulations and Voronoi grids, and 3D grids created by extrusion of 2D shapes (Lie et al., 2012). Unlike some other simulators, using grid geometry only in the preprocessor, MRST keeps the grid and petrophysical properties as individual entities. These entities serve as input for discretization in solvers and visualization modules.

Automatic differentiation is a technique that evaluates the derivative of a function and the calculation of this function. This technique is achieved by breaking down the function into a sequence of elementary arithmetic operations and elementary functions. And then, track each variable and apply chain rule repeatedly to obtain their derivatives along with the series of elementary calculations. Using automatic differentiation in reservoir simulators was first introduced in a commercial Intersect simulator, and then this technique is also implemented in many other simulators (DeBaun et al., 2005). By applying automatic differentiation, the Jacobian matrix in nonlinear Newton-Raphson iteration can be obtained implicitly during the calculation of residual equations. Therefore, it improves the accuracy and efficiency of the calculation. To implement automatic

differentiation in MATLAB, MRST uses operator overloading by creating user-defined classes with a relatively simple forward accumulation (Krogstad et al., 2015).

MRST also implements user-defined operators to create highly vectorized operators, including the discrete gradient and discrete divergence operator. The advantage of these discrete operators is that they are created with a sparse matrix, and therefore computations are done by efficient vector multiplications. Besides, as a result of making these discrete operators, the discretized equations could be written almost the same as the continuous partial differential equations. Examples of discrete operators are shown below:

$$div(v)\,[c] = \sum_{f \in F(c)} v[f]\; O_{\{c = N_1(f)\}} - \sum_{f \in F(c)} v[f]\; O_{\{c = N_2(f)\}}, \qquad (2.19)$$

where *div* is the discrete divergence; *v* is the discrete flux; *v[f]* is the flux only on face *f* with direction from $N_1(f)$ to $N_2(f)$; *c* is the cell that face *f* belongs to and $O_{\{expression\}} = 1$ if the expression is true otherwise it equals zero. The *div* operator is a linear mapping from faces to cells. Therefore, the discrete divergence of the fluxes from cell *c* represents the sum of all outgoing fluxes from the cell *c*. Similarly, the *grad* operator, mapping cells to their faces, is defined as the difference in cell values on the opposite side of the face:

$$grad(p)\,[f] = p\big[N_2(f)\big] - p\big[N_1(f)\big]. \qquad (2.20)$$

Besides, another operator, *avg*, that calculates the average of the cell values and its interior-connecting cell's value. These discrete operators are used for discretizing the partial differential equation from the previous section.

2.4. Discretization of Governing Equations for the Oil Phase

The following discretization uses notations in MRST and vectorized discrete operators that are introduced in the previous section. Then, from equation (2.7) and (2.10), the discrete oil phase equations are given by:

$$\frac{1}{\Delta t}\left(\phi(p[c])b_o(p[c])S_o[c]\right)^{n+1} - \frac{1}{\Delta t}\left(\phi(p[c])b_o(p[c])S_o[c]\right)^{n} + div\left(\vec{v}_o\right)[c]^{n+1} = \left(b_o q_o\right)[c]^{n+1}, \quad (2.21)$$

$$\vec{v}_o[f] = -upw\left(\Lambda_o\right)[f]T[f] \cdot \left(grad\left(p_o - p_{cow}\right)[f] - g\ avg\left(\rho_o\right)[f]grad(z)[f]\right). \quad (2.22)$$

where *c* and *f* denote cell values and face values; T[*f*] is the face-valued transmissibility, and p_{cow} is the capillary pressure between oil and water phase; similarly, *avg*(*p*)[*f*] is the face-valued pressure calculates the average pressure in two connecting cells; *upw* is the phase-upwind function, defined as,

$$upw\left(\Lambda_o\right)[f] = \begin{cases} \Lambda_o[N_1(f)], \text{if } grad\left(p_o - p_{cow}\right)[f] - g\,avg\left(\rho_o\right)[f]grad(z)[f] > 0 \\ \Lambda_o[N_2(f)], \text{otherwise.} \end{cases}, \quad (2.23)$$

and

$$\Lambda_o = \frac{b_o k_{ro}}{\mu_o}; \quad (2.24)$$

where b_o is shrinkage factor:

$$b_o = \frac{1}{B_o}; \quad (2.25)$$

2.5. Discretization of Governing Equations for the Gas Phase

The following discretization uses notations in MRST and vectorized discrete operators introduced in section 2.3. The gas component in the oil phase is included, and then, from the equation (2.9) and (2.10), the discrete water phase equations are given by:

$$\begin{aligned}&\frac{1}{\Delta t}\left(\phi(p[c])b_g(p[c])S_g[c]+\phi(p[c])b_o(p[c])S_o[c]R_s[c]\right)^{n+1}\\&-\frac{1}{\Delta t}\left(\phi(p[c])b_g(p[c])S_g[c]+\phi(p[c])b_o(p[c])S_o[c]R_s[c]\right)^{n}\\&+div\left(\vec{v}_g+\vec{v}_{go}\right)[c]^{n+1}=\left(b_g q_g+b_o q_o R_s\right)[c]^{n+1}\end{aligned}, \quad (2.26)$$

$$\vec{v}_g[f]=-upw\left(\Lambda_g\right)[f]T[f]\cdot\left(grad\left(p_g-p_{cgo}\right)[f]-g\ avg\left(\rho_g\right)[f]grad(z)[f]\right), \quad (2.27)$$

$$\vec{v}_{go}[f]=-upw\left(\Lambda_{go}\right)[f]T[f]\cdot\left(grad\left(p_o-p_{cow}\right)[f]-g\ avg\left(\rho_o\right)[f]grad(z)[f]\right), \quad (2.28)$$

where

$$\Lambda_g=\frac{b_g k_{rg}}{\mu_g}, \quad (2.29)$$

and

$$\Lambda_{go}=\frac{R_s b_o k_{ro}}{\mu_o}, \quad (2.30)$$

and the phase-upwind function, *upw*, is defined as,

$$upw\left(\Lambda_g\right)[f]=\begin{cases}\Lambda_g[N_1(f)], \text{if } grad\left(p_g-p_{cgo}\right)[f]-g\,avg\left(\rho_g\right)[f]grad(z)[f]>0\\ \Lambda_g[N_2(f)], \text{otherwise.}\end{cases}, \quad (2.31)$$

and

$$upw(\Lambda_{go})[f] = \begin{cases} \Lambda_{go}[N_1(f)], \text{if } grad(p_o - p_{cow})[f] - g\ avg(\rho_o)[f] grad(z)[f] > 0 \\ \Lambda_{go}[N_2(f)], \text{otherwise.} \end{cases}, \quad (2.32)$$

b_o and b_g are shrinkage factors:

$$b_g = \frac{1}{B_g}; \quad (2.33)$$

c and *f* denote cell values and face values; T[*f*] is the face-valued transmissibility, and p_{cwo} is the capillary pressure between water and oil phase. Similarly, *avg*(*p*)[*f*] is the face-valued pressure that calculates the average pressure in two connecting cells.

2.6. Discretization of Governing Equations for the Water Phase

The discretization of the water phase is like that of the oil phase, by using the notations in MRST and vectorized discrete operators introduced in section 2.3. Then, from equation (2.8) and (2.10), the discrete water phase equations are given by:

$$\frac{1}{\Delta t}\left(\phi(p[c]) b_w(p[c]) S_w[c]\right)^{n+1} - \frac{1}{\Delta t}\left(\phi(p[c]) b_w(p[c]) S_w[c]\right)^{n} + div(\vec{v}_w)[c]^{n+1} = (b_w q_w)[c]^{n+1}, \quad (2.34)$$

$$\vec{v}_w[f] = -upw(\Lambda_w)[f] T[f] \cdot \left(grad(p_w - p_{cwo})[f] - g\ avg(\rho_w)[f] grad(z)[f]\right), \quad (2.35)$$

where b_w is shrinkage factor; *c* and *f* denote cell values and face values; T[*f*] is the face-valued transmissibility, and p_{cwo} is the capillary pressure between water and oil phase; similarly, *avg*(*p*)[*f*] is the face-valued pressure calculates the average pressure in two connecting cells;

$$b_w = \frac{1}{B_w}; \quad (2.36)$$

$$\Lambda_w = \frac{b_w k_{rw}}{\mu_w}; \tag{2.37}$$

upw is the phase-upwind function, defined as,

$$upw(\Lambda_w)[f] = \begin{cases} \Lambda_w[N_1(f)], \text{if } grad(p_w - p_{cwo})[f] - g\,avg(\rho_w)[f]\,grad(z)[f] > 0 \\ \Lambda_w[N_2(f)], \text{otherwise.} \end{cases} \tag{2.38}$$

2.7. Discretization of Black-oil Equations in MRST

In MRST, the mass conservation equations of oil, gas, and water phase shown in the above sections are provided in the ad-black-oil module. The discretized equations are included in the black-oil solver as a function that assembles residual equations for conservation of oil, gas, and water, and Jacobians are provided by automatic differentiation.

For each Newton–Raphson iteration, the current and previous states of each grid block are obtained from solver where the phase velocity, formation volume factors, and upwind flags are also calculated, shown in figure 2.2. Then, these properties are used to assemble the mass conservation equations of each phase. For the black-oil model mentioned in section 2.1, the code for these equations is shown in figure 2.3, where water, oil, and gas in the figure are the accumulations terms and divWater, divOil, and divGas are the flux terms in the mass conservation equation. All the calculations are vector operations for all grids, and therefore assembles conservation equations for the whole reservoir model.

```
% Update state with AD-variables
state = model.setProps(state, {'s', 'pressure', 'rs', 'rv'}, {sat, p, rs, rv});
state0 = model.setProps(state0, {'s', 'pressure', 'rs', 'rv'}, {sat0, p0, rs0, rv0});
% Set up properties
state = model.initStateFunctionContainers(state);

[b, pv] = model.getProps(state, 'ShrinkageFactors', 'PoreVolume');
[b0, pv0] = model.getProps(state0, 'ShrinkageFactors', 'PoreVolume');
[phaseFlux, flags] = model.getProps(state, 'PhaseFlux',  'PhaseUpwindFlag');

[bW, bO, bG] = deal(b{:});
[bW0, bO0, bG0] = deal(b0{:});
[vW, vO, vG] = deal(phaseFlux{:});
[upcw, upco, upcg] = deal(flags{:});

[pressures, mob, rho] = model.getProps(state, 'PhasePressures', 'Mobility', 'Density');
```

Figure 2.2 Code for the Updating States in Black-Oil Equations.

```
% Upstream weight b factors and multiply by interface fluxes to obtain the
% fluxes at standard conditions.

bOvO = s.faceUpstr(upco, bO).*vO;
bGvG = s.faceUpstr(upcg, bG).*vG;

% The first equation is the conservation of the water phase. This equation is
% straightforward, as water is assumed to remain in the aqua phase in the
% black oil model.
bWvW = s.faceUpstr(upcw, bW).*vW;
water = (1/dt).*(pv.*bW.*sW - pv0.*bW0.*sW0 );
divWater = s.Div(bWvW);

oil = (1/dt).*(pv.*bO.*sO - pv0.*bO0.*sO0 );
divOil = s.Div(bOvO);

% The gas transported in the oil phase.
rsbOvO = s.faceUpstr(upco, rs).*bOvO;

gas = (1/dt).*(pv.* (bG.* sG  + rs.* bO.* sO) - ...
               pv0.*(bG0.*sG0 + rs0.*bO0.*sO0 ));
divGas = s.Div(bGvG + rsbOvO);
```

Figure 2.3 Code for Assemble Mass Conservation Equations in Black-Oil Equations.

3. WELL REPRESENTATION

In this section, the analytical solutions of the diffusivity equation for transient flow, pseudo-steady state flow, and steady-state flow are derived following Dake (1978). These equations describe the drawdown behavior in producing well in different states. The equations for well deliverability are also introduced following Economides et al. (2013).

3.1. Single Phase Radial Diffusivity Equation

The partial differential equation that describes the flow in porous media is called the diffusivity equation, which is derived from the mass continuity equation and Darcy's law and equation of state equation. Several assumptions are made to derive the radial flow diffusivity equation for the flow of a single fluid in homogenous formation, including Darcy's flow, isothermal condition, and constant compressibility.

The mass continuity equation is the mass balance within the porous media in which the mass accumulation rate is equal to the difference between the mass inflow rate and the mass outflow rate:

$$[\text{rate of Mass}]_{\text{inflow}} - [\text{rate of Mass}]_{\text{outflow}} = [\text{rate of Mass}]_{\text{accumulation}}. \quad (3.1)$$

For radial flow, the mass balance equation is:

$$\frac{\partial(q\rho)}{\partial r} = 2\pi r h \phi \frac{\partial \rho}{\partial t}. \quad (3.2)$$

Assuming horizontal flow and therefore dropping the gravity term, Darcy's law in radial form is given as

$$q = \frac{2\pi k h r}{\mu} \frac{\partial p}{\partial r}. \quad (3.3)$$

The isothermal compressibility can be expressed as

$$c = \frac{1}{\rho}\frac{\partial \rho}{\partial p}. \tag{3.4}$$

and differentiating with respect to time gives

$$\frac{\partial \rho}{\partial t} = c\rho \frac{\partial p}{\partial t}. \tag{3.5}$$

Substituting equation (3.3) and (3.5) in (3.2) gives

$$\frac{\partial}{\partial r}\left(\frac{2\pi hrk}{\mu}\rho\frac{\partial p}{\partial r}\right) = 2\pi hr\phi\rho c\frac{\partial p}{\partial t}. \tag{3.6}$$

Rearranging and simplifies to

$$\frac{1}{r}\frac{\partial}{\partial r}\left(\frac{\partial p}{\partial r}\right) = \frac{\phi\mu c}{k}\frac{\partial p}{\partial t}. \tag{3.7}$$

The equation above is the partial differential equation for single-phase radial flow in a porous medium. By applying the boundary condition and assumptions or special integration method, the diffusivity equation could be linearized for analytical solutions (Dake, 1978).

3.2. Single-phase Transient Flow

Transient flow is a relatively short period at the very beginning of the production after the change of pressure distributions occurs in the reservoir. Therefore, it's considered infinite acting because pressure distributions in the reservoir are not affected by the boundary. In transient flow, both pressure and pressure derivative are functions of both position and time, resulting in a relatively complex solution. Following Dake (1978), under several initial and boundary conditions, the diffusivity equation (3.7) could be solved using Boltzmann's transformation, giving

$$p(r,t) = p_i - \frac{q\mu}{4\pi kh} E_i(-x), \tag{3.8}$$

Where $E_i(-x)$ is the exponential integral and x is

$$x = \frac{\phi\mu c r^2}{4kt}. \tag{3.9}$$

When x is less than 0.01, which is sometimes the case, the exponential integral can be approximated as a function of -ln (γx) expressed as

$$E_i(-x) = -\ln(\gamma x) \quad \text{for } x < 0.01, \tag{3.10}$$

where γ is the exponential of Euler's constant and is equal to 1.781. Therefore, the pressure at the wellbore can be approximated as

$$p_{wf} = p_i - \frac{q\mu}{4\pi kh} \ln \frac{4kt}{\gamma\phi\mu c_t {r_w}^2}. \tag{3.11}$$

If the well is damaged and reduced in permeability in the damaged zone, the pressure drop will be larger. This additional pressure drop close to the well is defined by Van Everdingen (1953) with skin factor s as

$$\Delta p_{\text{skin}} = \frac{q\mu}{2\pi kh} s. \tag{3.12}$$

Including skin factor for transient flow, yields

$$p_{wf} = p_i - \frac{q\mu}{4\pi kh} \left(\ln \frac{4kt}{\gamma\phi\mu c_t {r_w}^2} + 2s \right). \tag{3.13}$$

and rearranging for the rate at the surface becomes

$$q_{sc} = \frac{4\pi kh(p_i - p_{wf})}{B\mu \left(\ln \frac{4kt}{\gamma\phi\mu c_t r_w^2} + 2s \right)}. \tag{3.14}$$

3.3. Single-Phase Pseudosteady-State Flow

The pseudo-steady-state condition indicates that a reservoir has been producing for a long enough time, and the pressure distribution is affected by the outer boundary. Therefore, at the boundary, the pressure is no longer constant but declines at a constant rate with time. The boundary conditions for pseudo-steady-state flow are shown below:

$$\frac{\partial p}{\partial r} = 0 \ \ at \ \ r = r_e , \tag{3.15}$$

$$\frac{\partial p}{\partial t} = \text{constant}, \ \ \text{for all} \ \ r \ \ \text{and} \ \ t . \tag{3.16}$$

By using the definition of compressibility, the material balance equation can be expressed as

$$cV\frac{dp}{dt} = -\frac{dV}{dt} = -q , \tag{3.17}$$

rearranging, and then substituting V for the radial volume we have,

$$\frac{dp}{dt} = -\frac{q}{c\pi r_e^2 h\phi} , \tag{3.18}$$

With the condition stated in the equation (3.16), substituting the equation (3.18) into the diffusivity equation (3.7) gives

$$\frac{1}{r}\frac{\partial}{\partial r}\left(\frac{\partial p}{\partial r}\right) = -\frac{q\mu}{\pi r_e^2 kh} , \tag{3.19}$$

integrating, and then gets

$$\frac{\partial p}{\partial r} = -\frac{q\mu r^2}{2\pi r_e^2 kh} + C_1 . \tag{3.20}$$

Using boundary condition (3.15) in (3.20) for C_1

$$C_1 = \frac{q\mu}{2\pi kh}, \tag{3.21}$$

substitutes in (3.20) and then rearrange to get

$$\frac{\partial p}{\partial r} = \frac{q\mu}{2\pi kh}\left(\frac{1}{r} - \frac{r}{r_e^2}\right). \tag{3.22}$$

Integrating (3.22) from r_e to r_w and including skin factor from the equation (3.12) gives

$$p_e - p_{wf} = \frac{q\mu}{2\pi kh}\left(\ln\frac{r_e}{r_w} - \frac{1}{2} + s\right). \tag{3.23}$$

The average reservoir pressure can be expressed as,

$$\overline{p} = \frac{\int_{r_w}^{r_e} p dV}{\pi\left(r_e^2 - r_w^2\right)h\phi} \approx \frac{\int_{r_w}^{r_e} p dV}{\pi r_e^2 h\phi}. \tag{3.24}$$

since $dV = 2\pi rh\phi$ we have

$$\overline{p} = \frac{2}{r_e^2}\int_{r_w}^{r_e} pr\ dr. \tag{3.25}$$

Combining (3.25) with (3.23) and complete the integral, we have

$$\overline{p} - p_{wf} = \frac{q_{sc}B\mu}{2\pi kh}\left(\ln\frac{r_e}{r_w} - \frac{3}{4} + s\right). \tag{3.26}$$

3.4. Single-phase Steady-State flow

The steady-state condition continued by the pseudo-steady-state flow that the well is completely open to the outer boundary. This condition assumes that the flow at the boundary balances the flow from the well. Therefore, the change of pressure over time is zero for all time and position. The boundary conditions are:

$$\begin{aligned} p_e &= \text{constant, } at\ r_e \\ \frac{\partial p}{\partial t} &= 0, \text{ for all r and t} \end{aligned}, \tag{3.27}$$

Then, the diffusivity equation (3.7) becomes

$$\frac{1}{r}\frac{\partial}{\partial r}\left(\frac{\partial p}{\partial r}\right) = 0, \tag{3.28}$$

Following Darcy's law equation (3.3), integrating

$$\int_{p_{wf}}^{p_e} dp = \frac{q\mu}{2\pi kh}\int_{r_w}^{r_e}\frac{dr}{r}. \tag{3.29}$$

$$p_e - p_{wf} = \frac{q\mu}{2\pi kh}\ln\frac{r_e}{r_w}. \tag{3.30}$$

Following a similar approach from the previous section, the average reservoir pressure could be obtained and given as,

$$\overline{p} - p_{wf} = \frac{q_{sc}B\mu}{2\pi kh}\left(\ln\frac{r_e}{r_w} - \frac{1}{2}\right). \tag{3.31}$$

3.5. Well deliverability

When wells are producing in stable regimes such as pseudo-steady-state flow and steady-state flow, the productivity index could be estimated to construct the inflow performance curve (IPR). The inflow performance curve represents the available pressure that the reservoir could deliver with the corresponding fluid flow rate. Outflow performance curve (OPR) relates the surface production rate with wellbore flowing pressure. It represents the required pressure for a well to deliver at a specific fluid flow rate from the reservoir to the surface. Combining IPR and OPR, the well deliverability could be found at the intersection of these two curves, also known as the operating point, as shown in figure 3.1.

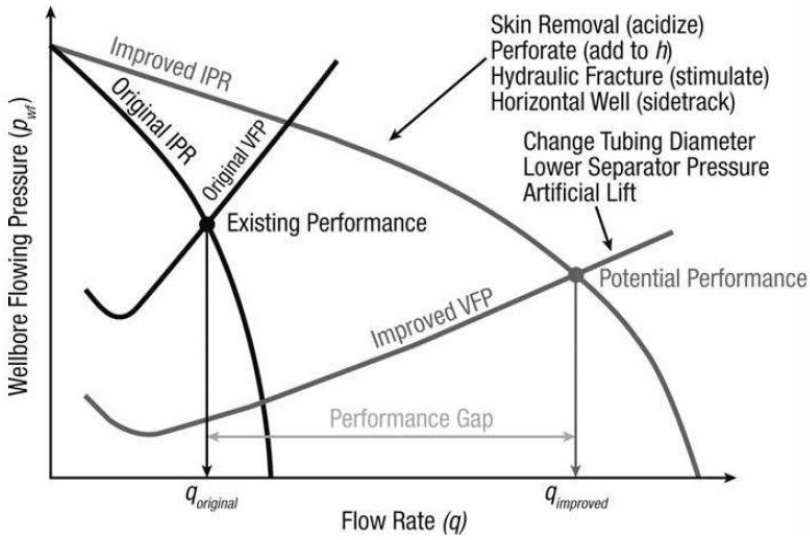

Figure 3.1 Well deliverability and optimized performance reprinted from (Economides et al. 2013).

The productivity index, J for oil wells could be represented with a general term for any production regime as

$$J = \frac{q_{sc}}{p - p_{wf}} = \frac{kh}{B\mu} J_D. \tag{3.32}$$

For Steady-State flow, from equation (3.31) and (3.30)

$$J_D = \frac{1}{\ln \frac{r_e}{r_w} + s},\ p = p_e. \tag{3.33}$$

$$J_D = \frac{1}{\ln \frac{r_e}{r_w} - \frac{1}{2} + s},\ p = \overline{p}. \tag{3.34}$$

For pseudo-steady-state flow, from equation (3.23) and (3.26)

$$J_D = \frac{1}{\ln \frac{r_e}{r_w} - \frac{1}{2} + s},\ p = p_e. \tag{3.35}$$

$$J_D = \frac{1}{\ln \frac{r_e}{r_w} - \frac{3}{4} + s},\ p = \overline{p}. \tag{3.36}$$

In reservoir simulation, the traditional IPR is based on Peaceman's equation (1978) in which reservoir pressure is estimated with well block pressure, the pressure of the grid containing the well. The traditional IPR calculation assumes steady-state radial flow of a single-phase fluid, and the productivity index and injectivity index are given by,

$$PI = \frac{q_{sc}}{P_{\text{block}} - \text{p}_{\text{wf}}}. \tag{3.37}$$

$$II = \frac{q_{sc}}{\text{p}_{\text{wf}} - P_{\text{block}}}. \tag{3.38}$$

The productivity index and injectivity index could be used to construct IPR to represent the deliverable pressure at a corresponding flow rate for production well, and required a corresponding flow rate for injection well, shown in figure 3.2.

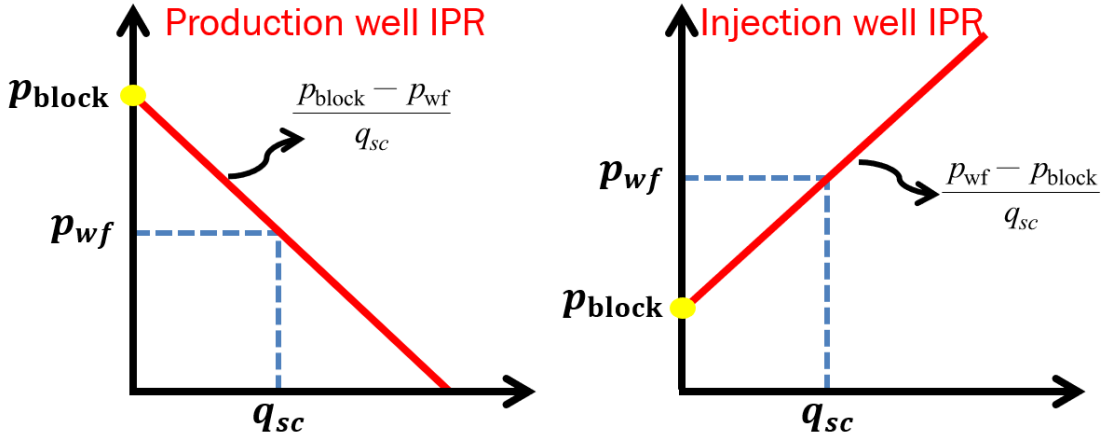

Figure 3.2 Well deliverability of production and injection well.

4. PROPOSED METHODOLOGY

In this section, the methodology for constructing IPR and OPR curves are discussed. The Beggs and Brill correlation is used to calculate the OPR curve following Beggs and Brill (1973, 1991). Following Jansen (2017), pressure in choke is calculated with multiphase choke empirical models. The design of the surface network model is shown with workflow charts.

4.1. Constructing the inflow performance curve (IPR)

4.1.1. IPR for Undersaturated Reservoir

IPR for the undersaturated reservoir is based on the application of both Darcy's law and Vogel's IPR, given by

$$q_o = q_{ob} + \left(q_{omax} - q_{ob}\right)\left(1 - 0.2\frac{P_{wf}}{\overline{P}} - 0.8\left(\frac{P_{wf}}{\overline{P}}\right)^2\right), \tag{4.1}$$

Where,

$$q_{ob} = J\left(\overline{P} - P_b\right), \tag{4.2}$$

$$q_{omax} = q_{ob} + \frac{JP_b}{1.8}. \tag{4.3}$$

The bubble point pressure Pb can be obtained from interpreting the PVT table or using fluid property correlations, such as Standing's black-oil correlation. This IPR is a combination of constant productivity IPR and Vogel's IPR and is shown in figure 4.1. There are two unknowns in this equation; One unknown is the average drainage area pressure $\overline{P}$, and another unknown is productivity index *J*.

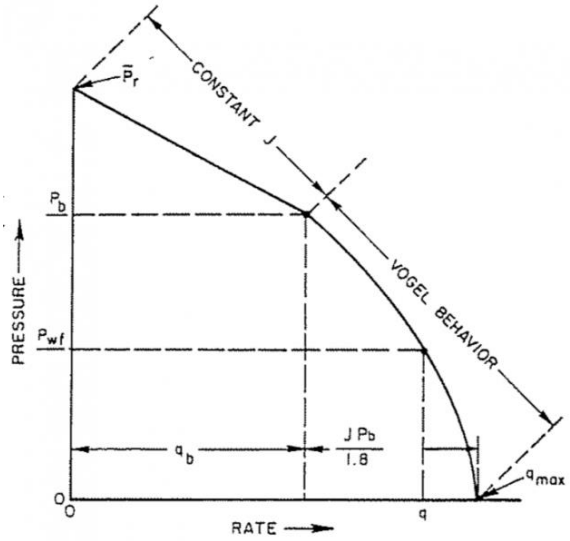

Figure 4.1 Combined single-phase liquid constant PI and Vogel's IPR reprinted from (Brown 1984).

4.1.2. IPR for Saturated Reservoir

IPR for the saturated reservoir is based on the application of Vogel's IPR, given by

$$q_o = q_{omax}\left(1 - 0.2\frac{P_{wf}}{\overline{P}} - 0.8\left(\frac{P_{wf}}{\overline{P}}\right)^2\right), \tag{4.4}$$

Vogel's IPR is the curve part of the undersaturated IPR, shown in figure 4.2. There are two unknowns in this equation; One unknown is the average drainage area pressure $\overline{P}$, and another unknown is the maximum rate *qmax*.

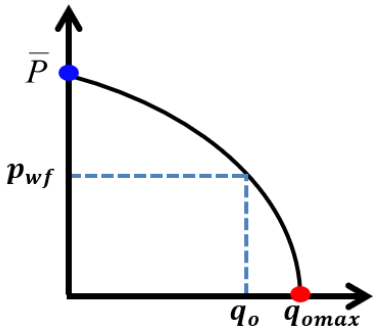

Figure 4.2 The Vogel's IPR.

4.1.3. IPR for Injection Well

Water injection is the only type of injection well used in this study. The IPR for injection well is based on Darcy's law, given by

$$q_w = II\left(\bar{P} - \mathrm{p_{wf}}\right), \tag{4.5}$$

There are two unknowns in this equation; One unknown is the average drainage area pressure $\bar{P}$, and another unknown is injection index *II*.

4.1.4. Method to Obtain IPR Functions

All three type of IPR used in this study contains two unknowns and therefore requires two equations to solve. The current operating point provides one equation. Thus, another operating point needs to be simulated. A very short simulation is performed after the current time step to construct IPR. The control for all wells is set to bottom-hole pressure at a value of 98% of current bottom-hole pressure. The flow rate is then obtained from the simulation, which will run for only one second to reduce the cost of simulation. Then, systems of equations in this section are solved, and the IPR could be obtained as a function of flow rate and used for coupling later with OPR. The scheme of this method is shown in figure 4.3.

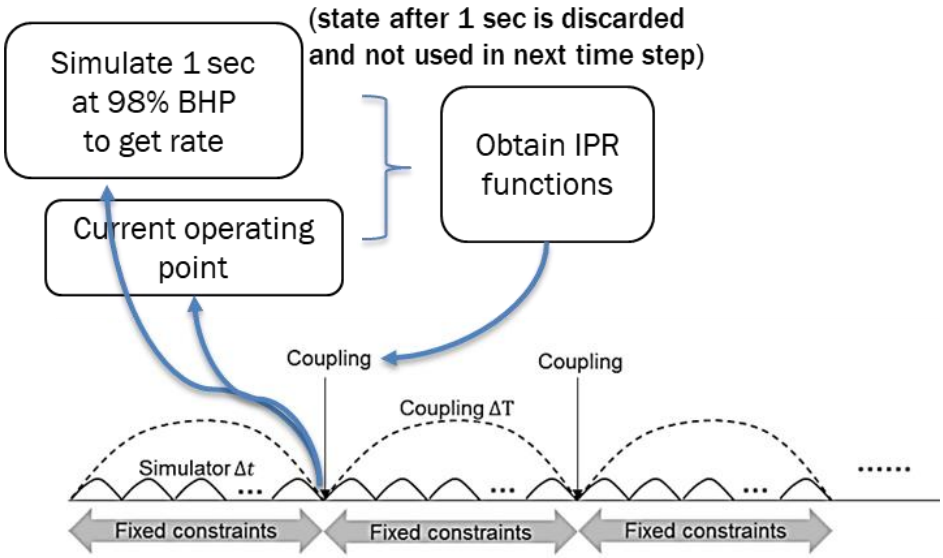

Figure 4.3 Method to Obtain the IPR Function.

4.2. Constructing the outflow performance curve (OPR)

Outflow performance curves are created to model the flow in the production system. The first step is to calculate fluid properties. In this study, the black-oil PVT model is used and is calculated with a series of correlations. Then, these fluid properties are inputs for the pressure drop calculation. The pressure drop in pipes is calculated with pressure traverse calculation with the energy balance equation.

$$\frac{dp}{dz} = \left(\frac{dp}{dz}\right)_{\mathrm{PE}} + \left(\frac{dp}{dz}\right)_{\mathrm{KE}} + \left(\frac{dp}{dz}\right)_{\mathrm{F}} \tag{4.6}$$

Empirical models, such as Beggs and Brill correlation and Mukherjee and Brill correlation, are used in analyzing multiphase flow through pipelines and wells. Beggs and Brill's correlation is shown in the next section.

4.2.1. Beggs And Brill Correlation

The pressure gradient equation used in Beggs and Brill correlation (Beggs and Brill, 1973) is:

$$-\frac{dp}{dz}=\frac{\frac{g}{g_c}\sin\theta\left[\rho_l H_L+\rho_g\left(1-H_L\right)\right]+\frac{f_{tp}G_m v_m}{2g_c d}}{1-\frac{\left[\rho_l H_L+\rho_g\left(1-H_L\right)\right]v_m v_{sg}}{g_c p}} \tag{4.7}$$

The mixture mass flux rate is $G_m=\rho_l v_{sl}+\rho_g v_{sg}$; the superficial gas, liquid, and mixture velocity is $v_{sg}=\frac{q_g}{A_p}$, $v_{sl}=\frac{q_l}{A_p}$ and $v_m=v_{sg}+v_{sl}$, where A_p is the pipe cross-section area and d is the pipe diameter.

The liquid holdup fraction H_L is calculated based on the determined flow pattern chart. The flow pattern chart is divided into four flow regimes: segregated, transition, intermittent, and distributed, bounded by the following correlation boundaries (Beggs and Brill, 1991):

$L_1=316\lambda_L^{0.302}$, $L_2=0.0009252$, $\lambda_L^{-2.4684}$, $L_3=0.10\lambda_L^{-1.4516}$, $L_4=0.5\lambda_L^{-6.738}$, where the no-slip liquid holdup is $\lambda_L=\frac{v_{sl}}{v_m}$, and the Froude number is $N_{FR}=\frac{v_m^2}{g\ d}$. The flow regime is determined by a set of inequalities in the following table:

Table 4.1 Flow regime boundaries for Beggs and Brill correlation.

Segregated	$\lambda_L<0.01$ and $N_{FR}<L_1$ or $\lambda_L\geqslant 0.01$ and $N_{FR}<L_2$
Transition	$\lambda_L<0.01$ and $L_2\leqslant N_{FR}\leqslant L_3$
Intermittent	$0.01\leqslant\lambda_l<0.4$ and $L_3<N_{FR}\leqslant L_1$ or $\lambda_l\geqslant 0.4$ and $L_3<N_{FR}\leqslant L_4$
Distributed	$\lambda_l<0.4$ and $N_{FR}\geqslant L_1$ or $\lambda_l\geqslant 0.4$ and $N_{FR}>L_4$

The flow regimes have the corresponding coefficient used to calculate liquid holdup, as shown in Table 4.2. The liquid holdup is calculated from $H_L = H_{L0}\psi$, where the liquid holdup at a horizontal position is $H_{L0} = \frac{a\lambda_L^b}{N_{FR}^c}$, and the inclination correction factor: $\psi = 1 + C\left[\sin(1.8\theta) - 0.333\sin^3(1.8\theta)\right]; \quad C = \left(1-\lambda_l\right)\ln\left(d\lambda_L^e N_{vl}^f N_{FR}^g\right)$, where the liquid velocity number is $N_{Lv} = v_{sl}\sqrt[4]{\frac{\rho L}{g\sigma_L}}$. For transition flow, the liquid holdup is calculated from both segregated and intermittent equations:

$$H_L = AH_{L_{Seg}} + (1-A)H_{L_{Int}}, \text{ where } A = \frac{L_3 - N_{FR}}{L_3 - L_2}. \tag{4.8}$$

Table 4.2 Beggs and Brill coefficients.

	a	*b*	*c*	
Segregated	0.98	0.4846	0.0868	
Intermittent	0.845	0.5351	0.0173	
Distributed	1.065	0.5824	0.0609	
	e	*f*	*g*	*h*
Segregated uphill	0.011	-3.768	3.539	-1.614
Intermittent uphill	2.96	0.3050	-0.4473	0.0978
Distributed uphill	C = 0 and ψ=1			
All patterns downhill	4.7	-0.3692	0.1244	-0.5056

For a smooth pipe, the no-slip friction factor is obtained from:

$$f_n = \left[2\log\left(\frac{N_{\mathrm{Re}_{ns}}}{4.5223\ \log\ N_{\mathrm{Re}_{ns}} - 3.8215}\right)\right]^{-2}, \tag{4.9}$$

where the Reynolds number is:

$$N_{\mathrm{Re}_{ns}} = \frac{\left[\rho_l\lambda_L + \rho_g\left(1-\lambda_L\right)\right]v_m d}{\mu_l\lambda + \mu_g\left(1-\lambda_L\right)}. \tag{4.10}$$

The two-phase friction factor is $f_{tp} = f_n e^S$, where

$$S = \frac{\ln(y)}{-0.0523 + 3.182\ln(y) - 0.8725\ln(y)^2 + 0.01853\ln(y)^4}, \qquad (4.11)$$

and $y = \frac{\lambda_L}{H_L^2}$, with constraint $S = \ln(2.2y - 1.2)$ when $1 \leqslant y \leqslant 1.2$.

4.2.2. Multiphase Choke Empirical Model

The pressure across the choke is calculated with empirical models, especially for multiphase flow, to avoid the computationally intensive iteration process. When chokes operate at critical conditions, the upstream pressure is independent of the downstream pressure. The upstream pressure of the choke at critical conditions is given by:

$$p_1 = -Aq_{l_{sc}} \frac{(ER_{gl})^B}{(Fd_{ch})^C} + D, \qquad (4.12)$$

where $q_{l_{sc}}$ is the liquid flow through the choke, R_{gl} is producing gas-liquid ratio, d_{ch} is the choke diameter and A, B, C, D, E, and F are coefficients for different empirical models, as shown in Table 4.3.

Table 4.3 Coefficients for different empirical choke model reprinted from (Jansen, 2017).

	SI Units					
Correlation	*A*	*B*	*C*	*D*	*E*	*F*
Gilbert	3.75×10^{10}	0.546	1.89	1.01×10^5	5.61	2.52×10^3
Ros	6.52×10^{10}	0.500	2.00	1.01×10^5	5.61	2.52×10^3
Baxendell	3.58×10^{10}	0.546	1.93	1.01×10^5	5.61	2.52×10^3
Achong	1.43×10^{10}	0.650	1.88	1.01×10^5	5.61	2.52×10^3
	Field Units					
Correlation	*A*	*B*	*C*	*D*	*E*	*F*
Gilbert	10.0	0.546	1.89	14.7	1.00	1.00
Ros	17.4	0.500	2.00	14.7	1.00	1.00
Baxendell	9.56	0.546	1.93	14.7	1.00	1.00
Achong	3.82	0.650	1.88	14.7	1.00	1.00

When upstream pressure p_1 is below approximately 1.7 times the downstream pressure p_4, the choke is operating at sub-critical conditions other than the critical condition (Jansen, 2017). The empirical model for sub-critical flow is derived from the critical model with several boundary conditions. From the equation (4.12), the flow rate at the critical pressure is given by:

$$q_{l_{sc},crit} = \frac{\left(D - p_{1,crit}\right)\left(Fd_{ch}\right)^{C}}{A\left(ER_{gl}\right)^{B}}, \tag{4.13}$$

where $p_{1,crit} \approx 1.7p_4$. At sub-critical conditions, the upstream pressure is provided by:

$$p_1 = p_4 + c_2 q_{l,sc}^2 + c_3 q_{l,sc}^3, \tag{4.14}$$

where

$$\begin{aligned} c_2 &= \frac{p'_{1,crit}}{2q_{l_{sc},crit}} + \frac{3\left(p_{1,crit} - \frac{1}{2}p'_{1,crit}q_{l_{sc},crit} - p_4\right)}{q_{l_{sc},crit}^2} \\ c_3 &= -\frac{2\left(p_{1,crit} - \frac{1}{2}p'_{1,crit}q_{l_{sc},crit} - p_4\right)}{q_{l_{sc},crit}^3} \end{aligned}, \tag{4.15}$$

and $p'_{1,crit} = -A\dfrac{\left(ER_{gl}\right)^{B}}{\left(Fd_{ch}\right)^{C}}$.

4.2.3. Pressure Traverse Calculation

The traditional pressure traverse calculation is an iterative process. The total distance is divided into fixed-length segments, which are sufficiently small to consider constant fluid properties and pressure gradient. The pressure drop in each segment is calculated by trial and error in which the fluid properties are calculated with an

approximate pressure drop. Then, the pressure gradient is calculated to obtain a new pressure drop to compare with the initial guess (Economides et al., 2013).

In this study, the pressure traverse calculation is replaced by numerical integration of equation (4.7), the pressure gradient equation. MATLAB's ODE45 built-in nonstiff solver could be used to solve the problem with inputs of pressure and total distance. The accuracy of the result could be checked by repeating the numerical integration in the opposite direction (Jansen, 2017).

4.3. Explicit Coupling and Optimization

In the optimization process of the production wells, the outflow performance curve (OPR) and the inflow performance curve (IPR) are constructed at the end of each time-step. OPR is built by iterating the pressure traverse calculation at a range of flow rates; IPR is created with simulation results from the reservoir simulator. Then, the optimal operating point for production wells can be obtained from the intersection of the inflow and outflow performance curve, shown in figure 4.4. This operating point will be used as a well constraint in the next reservoir simulation. For injection wells, the well will operate at maximum bottom-hole pressure unless the rate is larger than the maximum injection rate. Instead, the injection well will operate at the maximum rate.

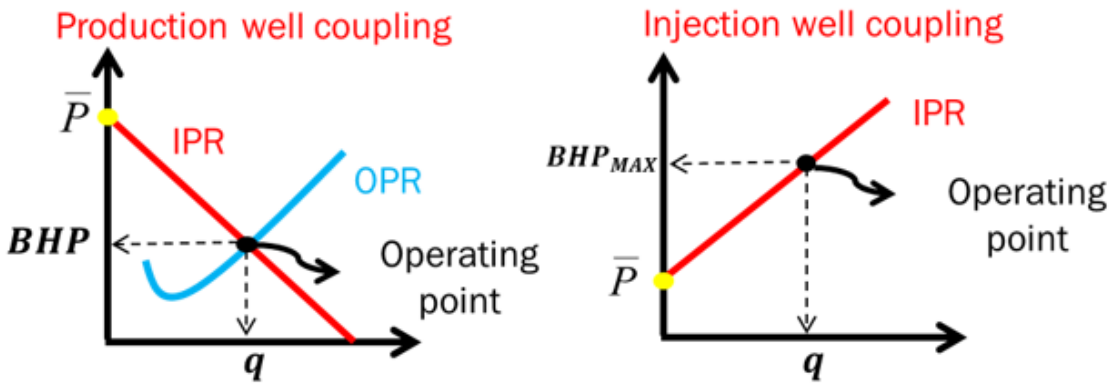

Figure 4.4 Explicit Coupling for Production and Injection Wells.

In this study, the operating point for production well coupling is obtained by a modified bisection method, nth section method. The bisection method is an approximation method that iteratively divides an interval that contains a root of the function. In each iteration, the bisection divides the interval by half and select the half interval that includes the root. The process continues until the difference between the function is smaller than the tolerance. The modified bisection method divides the interval into multiple sections instead of two to reduce iterations (Rivaie, 2017). This method is easy to use and apply, and the number of iterations is not high, with a reasonable amount of computational cost.

Finally, after performing analysis on multiple wells at the end of each time step in reservoir simulation, new operating points are obtained. Then, update each well constraint in the reservoir simulation corresponding to the optimal operating point for the next time-step and perform reservoir simulation for the next time step. Repeat the process above until the end of the time step. And finally, the production system is explicitly coupled and optimized with the reservoir at the end of each time-step. The workflow of the whole coupling and optimization process is shown in Figure 4.5 and Figure 4.6.

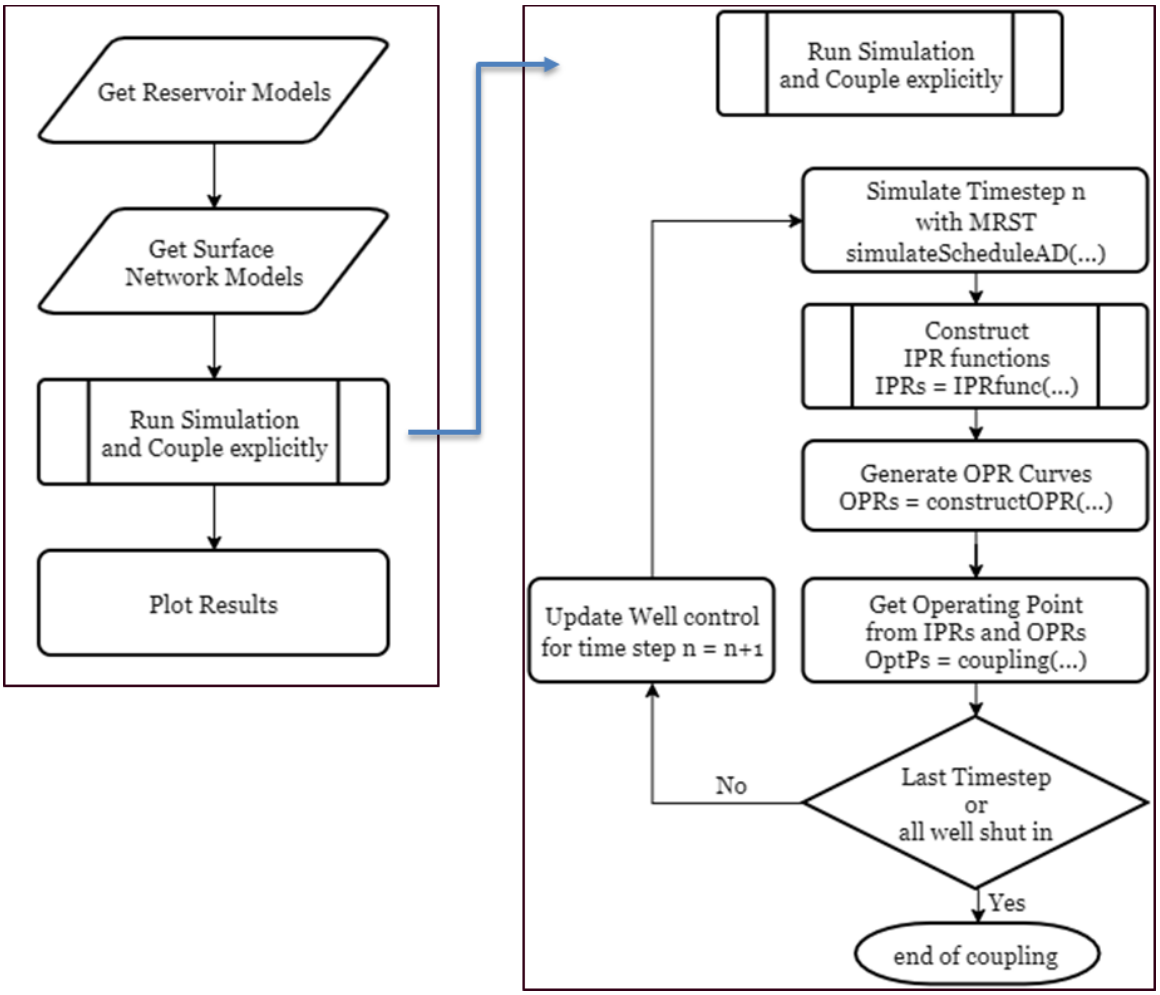

Figure 4.5 Flow chart for explicit coupling.

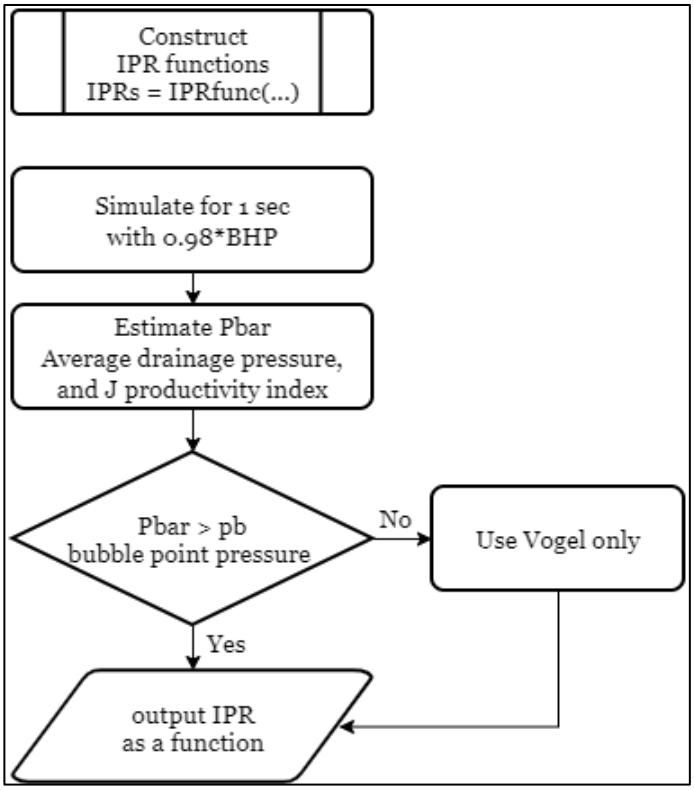

Figure 4.6 Flow chart for IPR functions.

4.4. Surface Coupling Module Design

The surface coupling module is designed to be user friendly while maintaining high efficiency. At this stage, the interface has not been made because it's not efficient to input data with the interface. The typical workflow of this module in MATLAB is shown in the top left part of figure 4.5, which includes setting the reservoir model and surface model and running the explicitly coupled simulation.

In this study, the configuration of reservoir simulation for the UNISIM model is the same as the default setting in the 2020a version of MRST's initEclipsePackedProblemAD function, which sets up a packed problem based on Eclipse input with reasonable defaults. The sample code setting up the UNISIM model for reservoir simulation is shown in the upper section of figure 4.7. The outputs of the first section, "model", "initState", and

"schedules" are the original MRST structures, which will be used as input for constructing the surface network structure, shown in the lower section of figure 4.7.

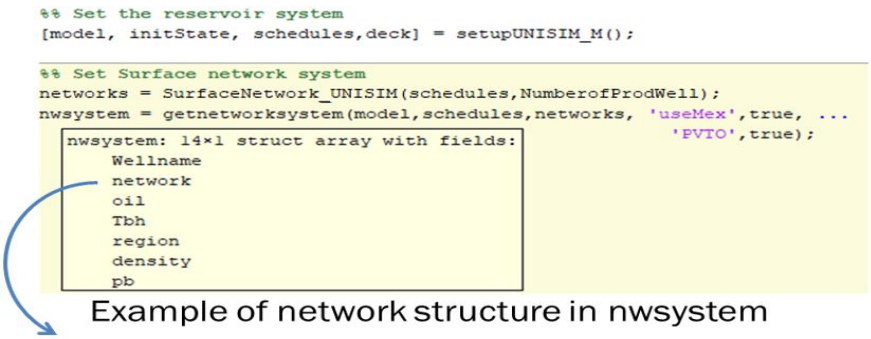

nwsystem(1).network

Fields	name	type	model	diameter	inclination	roughness	length	T_bottom	Psep
1	'Separator'	[]	[]	[]	[]	[]	[]	20	6.8948e+05
2	'Riser'	1	1	0.1524	0	3.0000e-05	166	40	[]
3	'Flowline'	1	1	0.1524	1.5708	3.0000e-05	1045	70	[]
4	'Tubing'	1	1	0.1143	0	3.0000e-05	2.7959e+03	80	[]

Figure 4.7 Data Format for Surface Network.

The "getnetworksystem" function will output a network system structure for each production well with seven fields, including "Wellname", "network", "oil", "Tbh", "region", "density", and "pb". The network field is also a structure that stores components of the surface network for each well. An example of a network structure is shown in figure 4.7. In network structure, the type field is defined as the type of components, and currently, there are two types of components where 1 is for pipe segments, such as tubing and flowline, and 2 is for chokes. In the network structure, the model field is defined as the model used for the pipe segment and choke. Currently, there are three types of pipe models and four types of choke models available. All the pipe and choke models are empirical models. The model number and its corresponding model are shown in table 4.4. All input units for the coupling modules are SI units and the inclination field in radians.

Table 4.4 Pipe and Choke Correlations for Model Field in Network Structure.

Model	Pipe Correlations	Choke Correlations
1	Beggs and Brill	Gilbert
2	Mukherjee and Brill	Ros
3	Hagedorn and Brown	Baxendell
4		Achong

In the network system structure, the user input fields include "oil", "Tbh", and "region". The oil field is defined as the type of black-oil correlation used for fluid properties where 1 is for Standing, and 2 is for Glaso; The Tbh field is defined as the bottom-hole temperature; The region field is defined as the reservoir region where the well is located. The density and pb fields are the outputs of the function. The option "PVTO" is defined as the method to determine the bubble point pressure where true is for interpreting the PVTO table, and false is for using empirical correlations. After obtaining the surface network system, the explicitly coupled simulation could be done using the function "Surface_coupling" to get a result structure shown in figure 4.8.

```
%% Surface coupling
Results = Surface_coupling(initState, model, schedules, nwsystem, ...
                                                    'usePblock',false, ...
                                                'nonlinearsolver',nls, ...
                                                     'IPRsolver',nls1, ...
                                                     'oldresults',[]);
```

```
Results:
  struct with fields:

          Tstep: [10×1 double]
          OptPs: {10×1 cell}
           OPRs: {10×1 cell}
        INJIPRs: {10×1 cell}
           IPRs: {10×1 cell}
          WSols: {10×1 cell}
    Elapsedtime: [10×3 double]
            STs: {11×1 cell}
```

```
%% plot solutions
plotWellSols(Results.WSols,Results.Tstep);
```

Figure 4.8 Explicit Coupling and Plotting in MRST.

The results structure contains all the IPR and OPR curves and their intersection points, which are the optimum points denoted as OptPs. The result also includes the simulated time steps represented by Tstep, the well solutions at each time step denoted as WSols, the reservoir grid blocks solutions denoted as STs, and the total elapsed time for the simulation denoted as Elapsedtime. With well solutions and simulated time steps, the well solutions can be plotted with MRST's interactive plotting interface, the "plotWEllSols" function, shown in the lower section of figure 4.8.

5. ASSESSMENT OF THE PROPOSED METHODOLOGY

5.1. Applications

In this section, the explicit coupling is performed on two models. One is a simplistic "shoe-box," and another is a complex model, UNISIM, based on a real offshore field.

5.1.1. The Simplistic Reservoir Model

The simplistic reservoir model is an undersaturated and closed boundary reservoir with an area of 10,000 meters by 10,000 meters, divided into 41 by 41 grids, and 30 meters in thickness, divided into three layers. The reservoir is homogenous and anisotropic only in vertical permeability. The reservoir has an initial pressure of 5,000 psia. This reservoir has one production well and one injection well, and both are 13 grids away from each other and the closest boundary, shown in figure 5.1. The injection well is not coupled, operating at a constant pressure of 5,000 psia. The production well has a maximum surface oil rate of 8,000 STB/day and minimum bottom-hole pressure of 2500 psia.

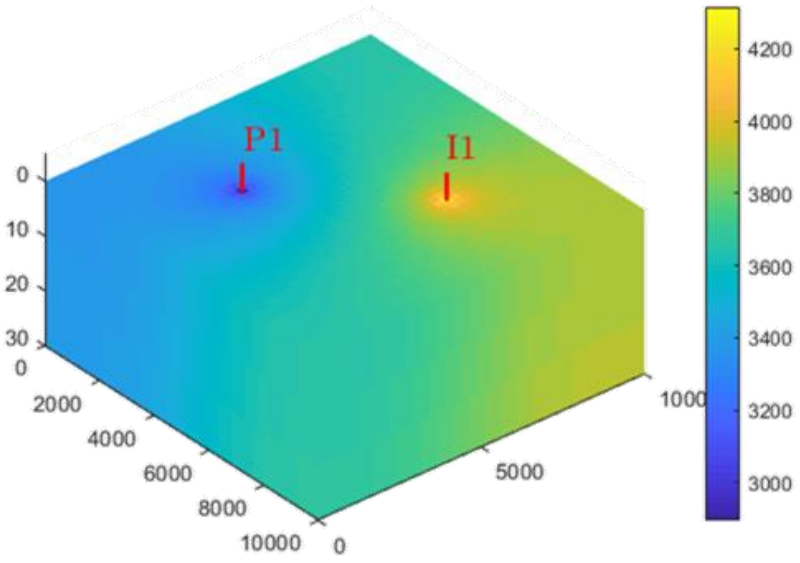

Figure 5.1 The Simplistic Reservoir Model.

5.1.2. The Surface Model of the Simplistic Model

The surface network model for production well P1 simplistic model contains a tubing, a choke, and a flowline, shown in figure 5.2. A sample of pressure traverse is generated at the initial water cut and the gas-oil ratio at a rate of 3500 STB/day, shown in figure 5.3.

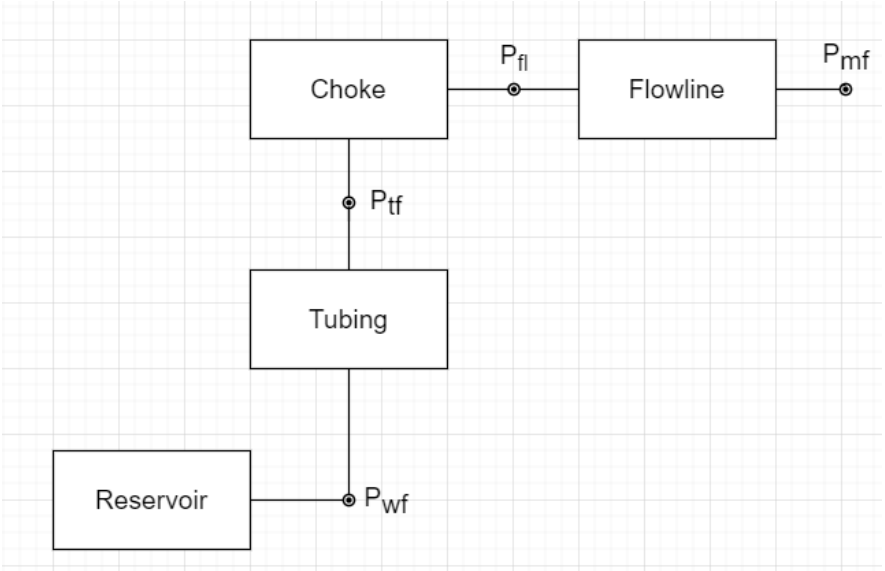

Figure 5.2 Surface Network for Simplistic Model.

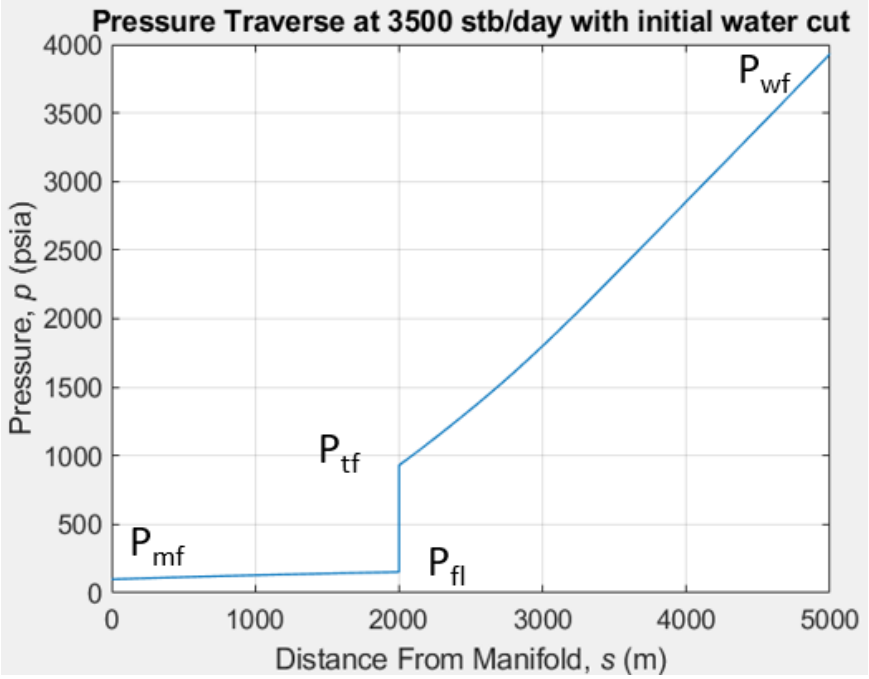

Figure 5.3 Pressure Traverse Calculation for Simplistic Model.

5.1.3. Simulation of the Simplistic Model without Coupling

To demonstrate the effect of coupling, the simplistic model is simulated without coupling, and the resulting bottom-hole pressure and surface oil rate are shown in figure 5.4.

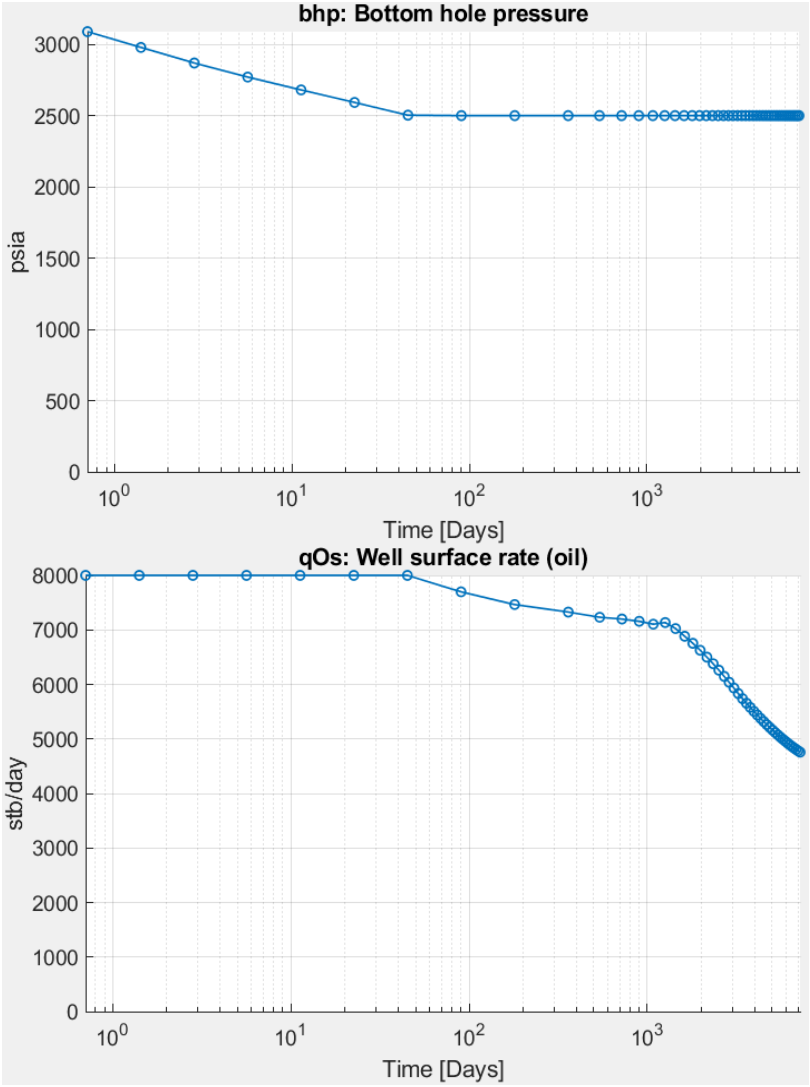

Figure 5.4 Surface Oil Rate and BHP of P1 in the Simplistic Model, without Coupling.

The production well P1 is producing at a maximum rate until the minimum bottom-hole pressure is reached. The reservoir simulation only shows the rate at the bottom hole, and the actual surface oil rate has to be obtained with OPR. A pressure traverse calculation is performed to check the required pressure at a maximum flow rate of 8000 STB/day that

is 5376 psia of wellbore flowing pressure, shown in figure 5.5. However, in figure 5.4, the available bottom-hole pressure is less than 3000 psia. As a result, there would be no production at the surface network.

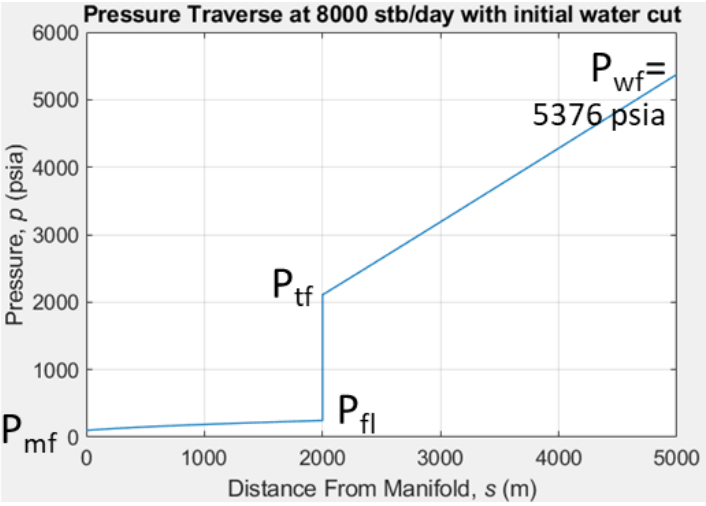

Figure 5.5 Pressure Traverse Calculation at The Maximum Rate.

5.1.4. Simulation of the Simplistic Model with Coupling

To show the coupling process, IPR and OPR are plotted along with the previous and next operating point, shown in figure 5.6. The result of the coupled simulation is shown in figure 5.7.

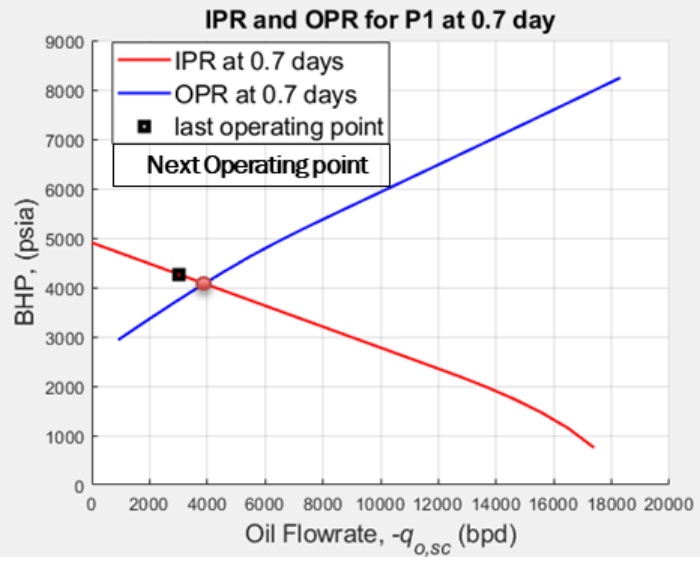

Figure 5.6 Well deliverability of p1 on 0.7 days.

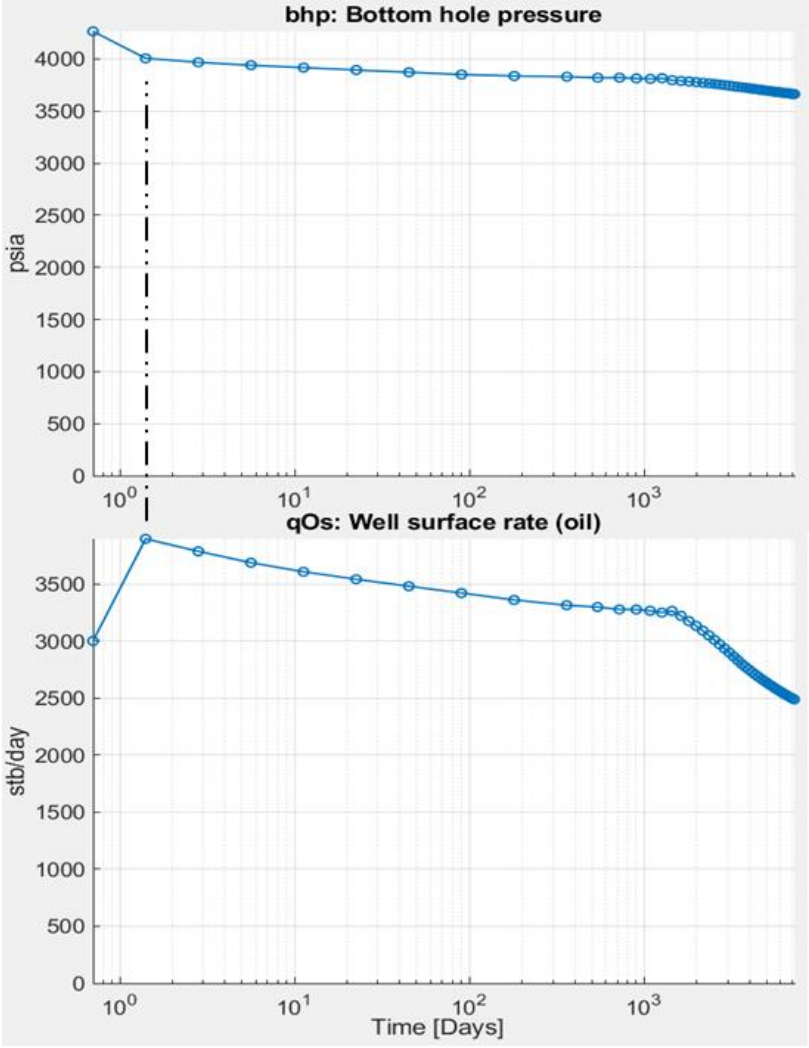

Figure 5.7 Surface Oil Rate and BHP of P1 in the Simplistic Model, With Coupling.

Initially, the production rate was 3000 STB/day. After coupling the first production rate, a new operating point at around 4000 STB/day is obtained and is used for the next simulation, the operating point shown with the dashed line in figure 5.7. The total simulation time is 7200 days, and the maximum time step size is 180 days. The result of surface network coupling is stable, with no sign of oscillation.

5.1.5. Analysis of the Coupling result of the Simplistic Model

There are two different decline rates observed in the surface oil rate of the production well in figure 5.7. An analysis is performed at three time-steps to determine the reason for the change in decline rates. These three time-steps are shown in figure 5.8, and two points are analyzed at a time to check what factors contribute to each decline rate.

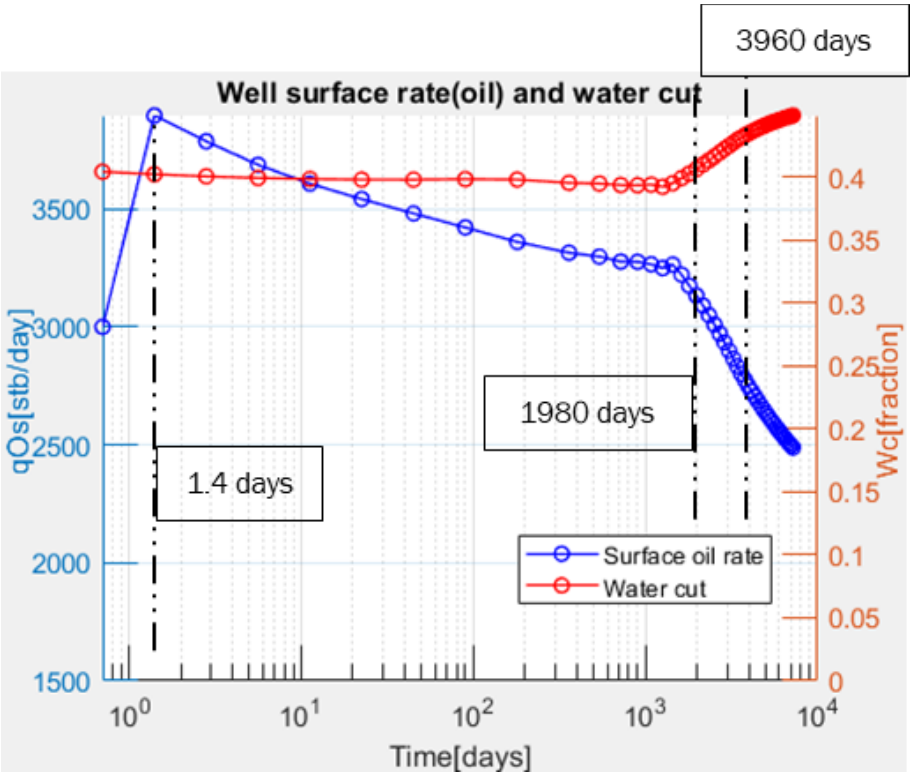

Figure 5.8 Oil Rate and Water Cut of the Production Well.

In order to check the factors for the first decline rate, the IPR and OPR curves in 1.4 days and 1980 days are plotted, shown in figure 5.9. The OPR curve for these two points almost overlapped with not much difference. The IPR curve is shifted downward from 1.4 days to 1980 days because of the decrease in drainage area pressure. Therefore, the decline in drainage area pressure is the leading cause of the first decline rate.

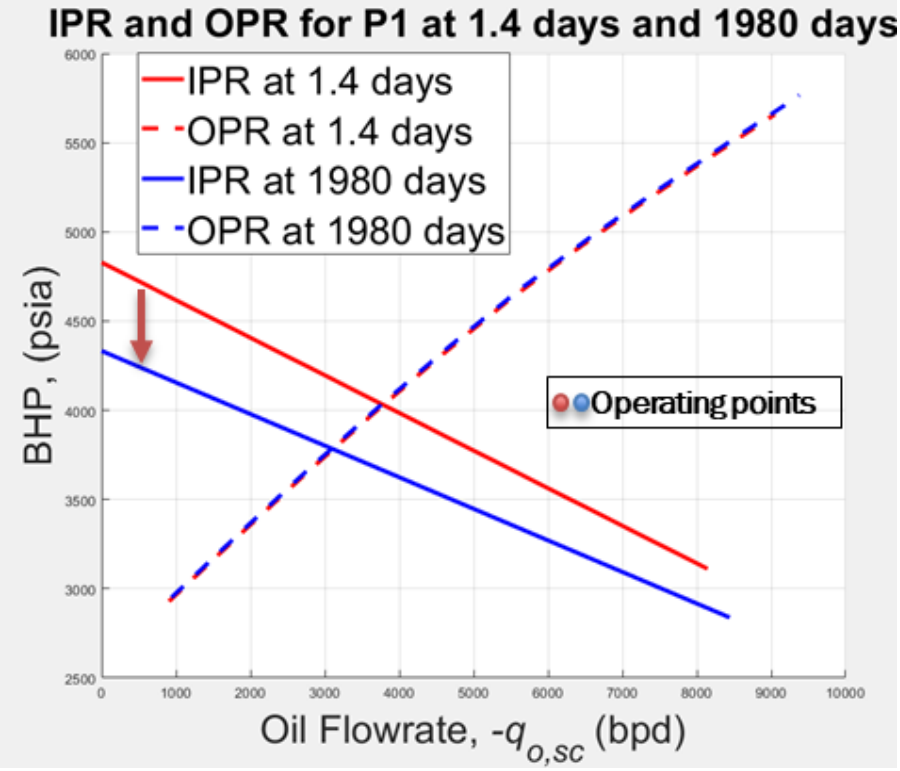

Figure 5.9 IPR and OPR Curves for Production Well at first two points.

In order to check the factors for the second decline rate, IPR and OPR curves in 1980 days and 3960 days are plotted, shown in figure 5.10. The OPR curve is shifted upward because of the increase in water cut where the liquid density increases and requires higher pressure to transport them to the surface. The IPR curve is shifted downward because of the decrease in drainage area pressure. Therefore, the decrease in drainage area pressure and increase in water cut are the main causes of the second decline rate.

The results of the surface coupling in the simplistic model can be explained and are expected. Also, there is no oscillation observed in this application. Next, the surface coupling is applied in a complicated model in the next section.

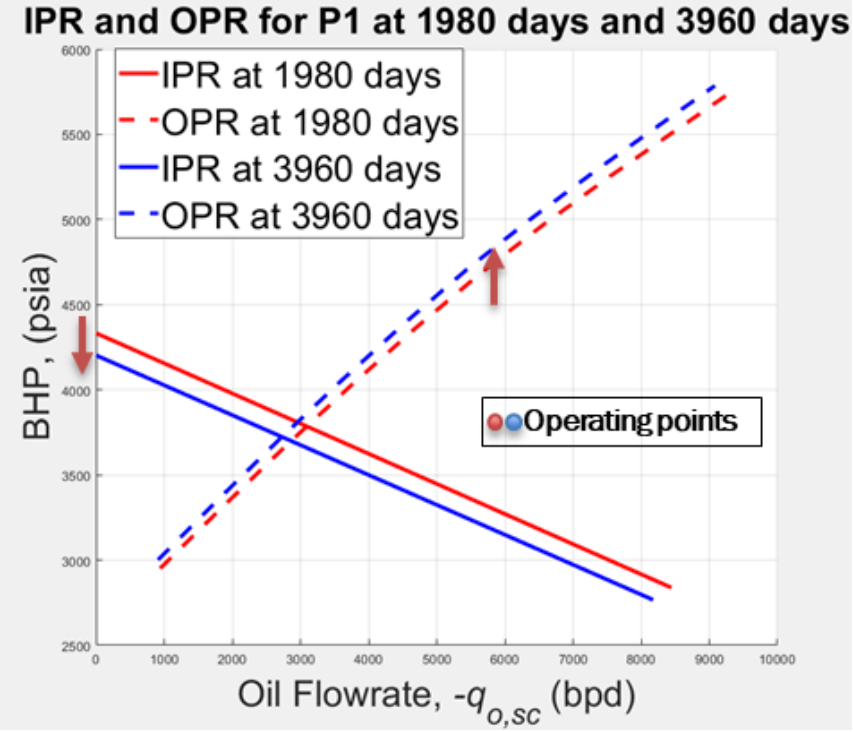

Figure 5.10 IPR and OPR Curves for Production Well at last two points.

5.1.6. The UNISIM Model

The UNISIM-I-D Model is based on Namorado Field, an offshore field in Campos Basin, Brazil. The reservoir model has a total of 81x58x20 grid blocks, where each grid block has a dimension of 100x100x8 meters (Figure 5.11).

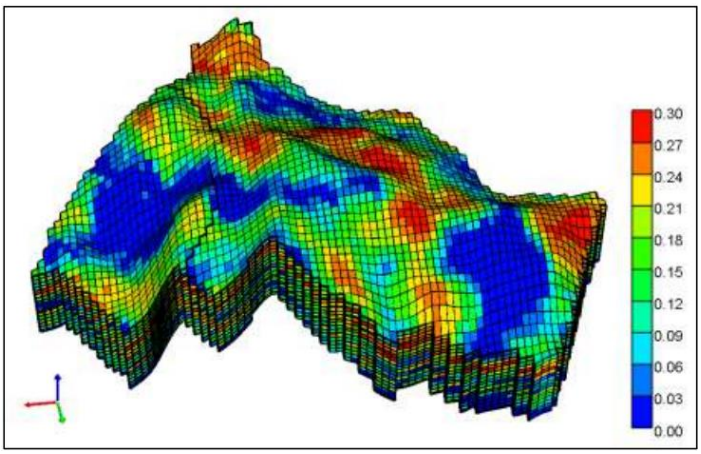

Figure 5.11 UNISIM-I-D: Porosity Map reprinted from (Gurjão, 2018).

The UNISIM-I-M model holds the same assumption as UNISIM-I-D, where the reservoir is undersaturated and using a black-oil fluid model, with the same reservoir model. The UNISIM-I-M model has 11 horizontal injection wells,10 horizontal production wells, and 4 vertical production wells (Figure 5.12).

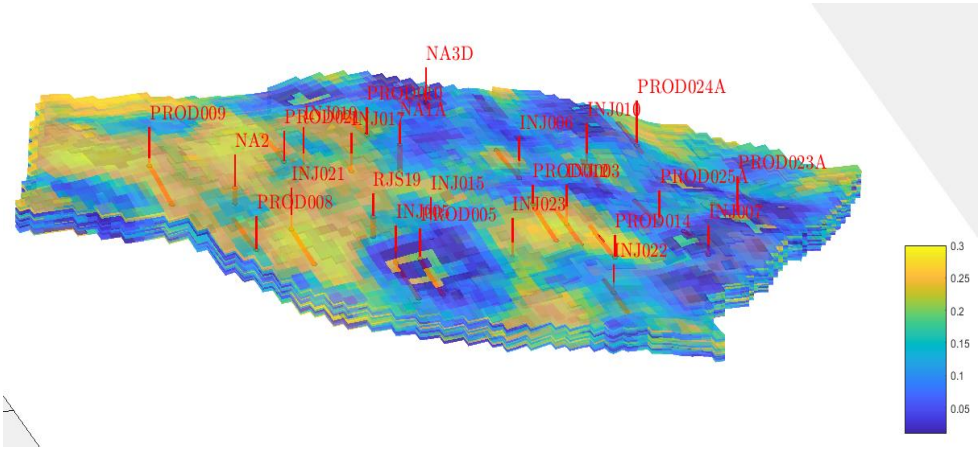

Figure 5.12 UNISIM-I-M: Well Placement.

A Basic reservoir model description for UNISIM-I-D is shown in table 5.1. The detailed reservoir description could be found in the work of Avansi & Schiozer (2015).

Table 5.1 Basic reservoir description for UNISIM-I-D/M reprinted from (Gurjão, 2018).

Reservoir data	Value	Units
Depth	2900-3400	m
Water depth	166	m
Coastline distance	80	km
Water temperature	20 to 16 linear (downhill)	ºC
Sea current	0.5	m/s

5.1.7. The Surface Model of the UNISIM Model

The surface network model for all production wells in UNISIM contains the same components in the same diameter; however, different lengths, shown in figure 5.13 and table 5.2. The surface model for each well includes a production tubing, a flowline, and a riser.

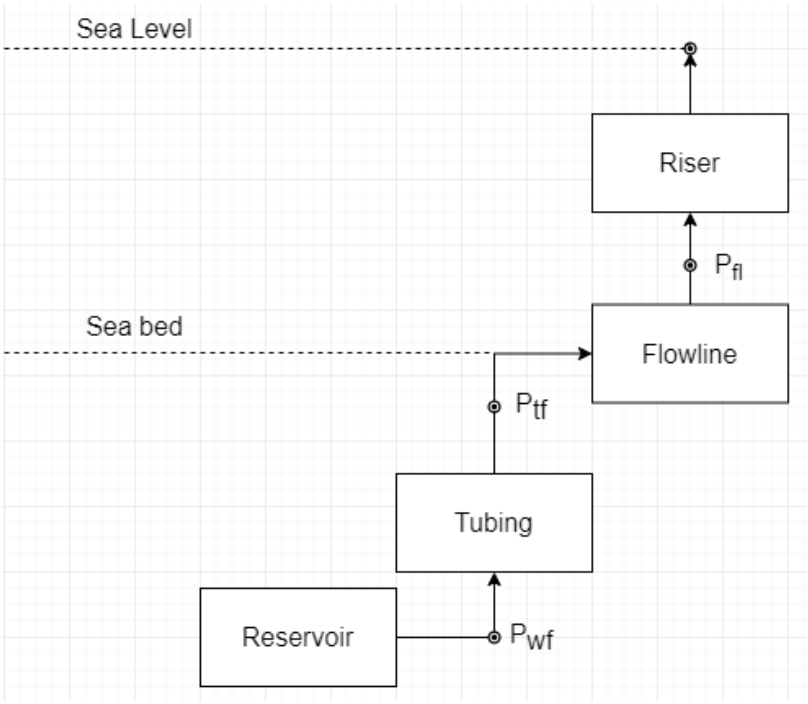

Figure 5.13 Surface Network for Each Well in UNISIM.

Table 5.2 Wellbore and Pipe Segment Diameter for UNISIM.

	Diameter
Riser	6 in
Flowline	6 in
Tubing	4.5 in
Wellbore	6 in

5.1.8. Simulation of the UNISIM Model without Coupling

To show the effect of coupling, the simplistic model is simulated without coupling, and the resulting bottom-hole pressure and surface oil rate are shown in figure 5.14.

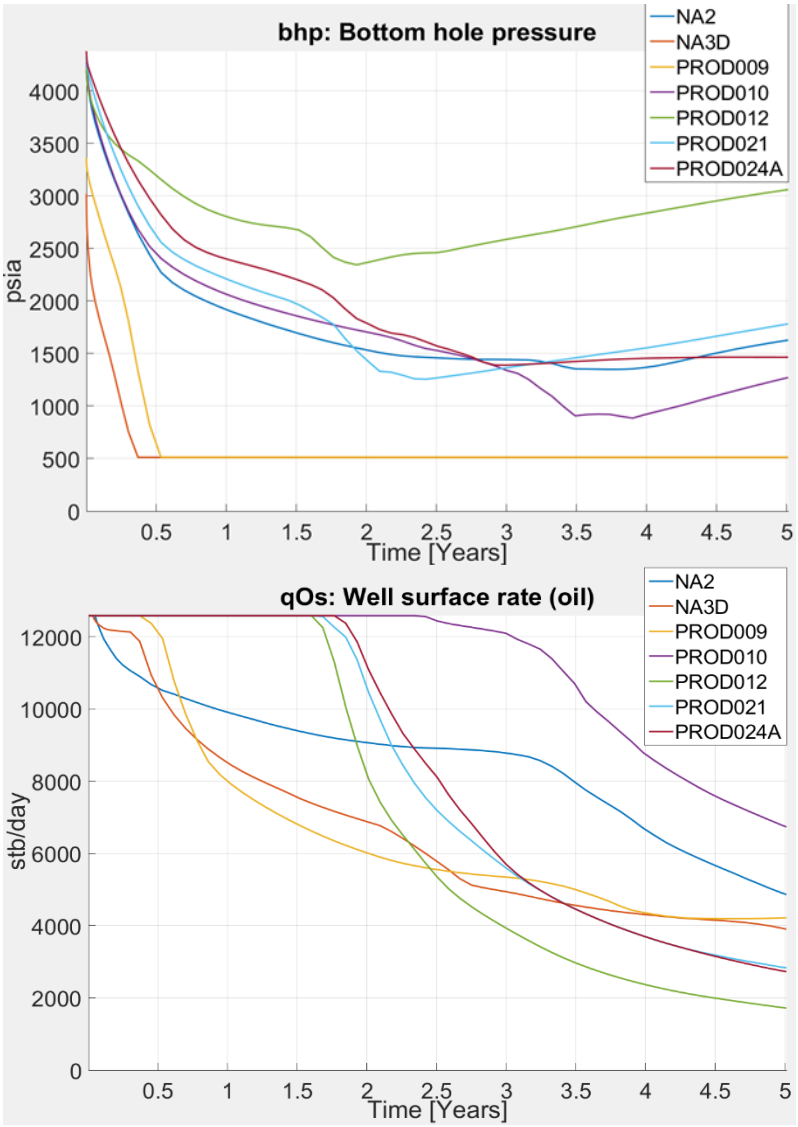

Figure 5.14 Surface Oil Rate and BHP of production wells without Coupling in UNISIM.

Similar to the simplistic model, the production wells are producing at a maximum rate until the minimum bottom-hole pressure is reached. The reservoir simulation only shows the rate at the bottom hole, and the actual surface oil rate has to be obtained with OPR. The minimum bottom-hole pressure for all the production wells is about 500 psia,

which too small to transport flow to the surface, and therefore there would be no production at the surface network.

5.1.9. Simulation of The UNISIM Model with Coupling

All the production wells and injections wells in the UNISIM model are coupled at 1-day, 15-day, 30-day interval and then coupled every 60 days. The increment of time-step size at the beginning of the simulation allows faster convergence to improve accuracy and reduce the number of iterations for each Newton iterations. The result for production wells is shown in figure 5.15. There are no apparent oscillations observed from results in the production wells or injection wells (figure 5.16).

Both the UNISIM model and the simplistic model shows stable results with no oscillations even with a considerable coupling period. However, after using the traditional IPR calculation, similar results are obtained with no oscillations. Additional analysis is discussed in the next chapter.

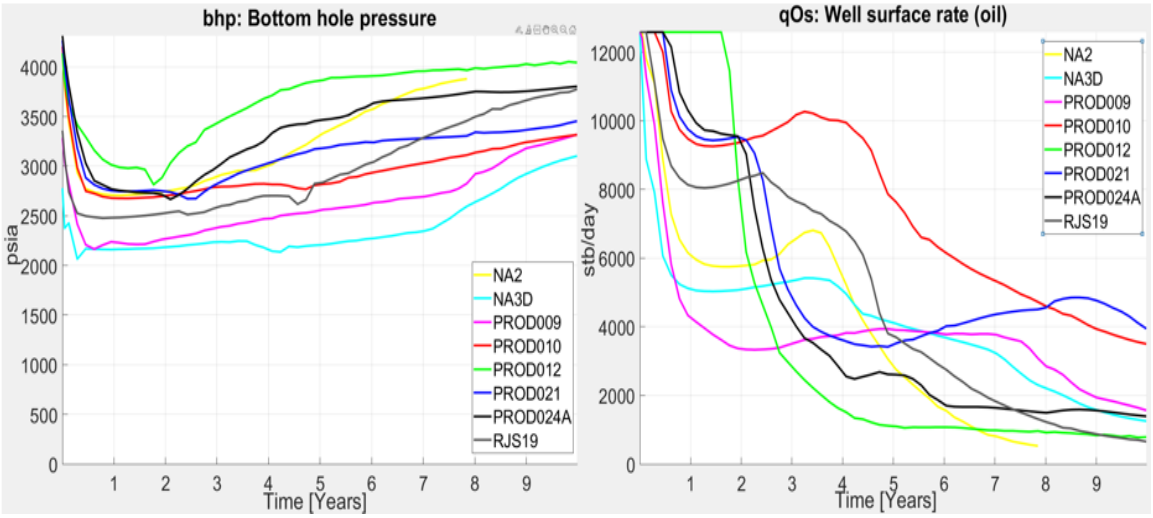

Figure 5.15 Surface Oil Rate and BHP of production wells with Coupling in UNISIM.

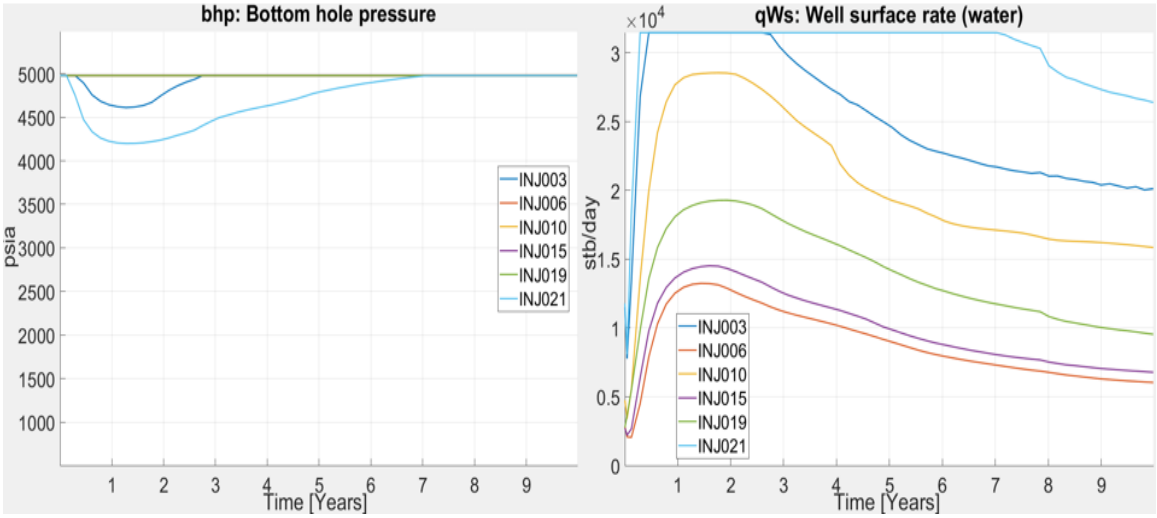

Figure 5.16 Surface Water Rate and BHP of Injection wells with Coupling in UNISIM.

5.1.10. Computational Cost of Coupling the UNISIM Model

The average computational cost for each time step of coupling is shown in table 5.3. The cost to construct the IPR curve with the new method is only 7 seconds, which is very low comparing to the reservoir simulation cost. The cost to build the OPR curve is reasonable, considering a total of 14 production wells.

Table 5.3 Computational Cost of Coupling UNISIM Model.

Simulation cost				
	1 day	15-days	30-days	60-day
Average Time(sec)	28	178	57	58
	IPR cost		OPR cost	
Average Time(sec)	7		20	

5.2. Results and discussions

In chapter 5, the application of toolbox demonstrates the use of the explicit coupling method for the simplistic and complex model. However, no oscillation was observed. In this section, results using well block pressure are compared with results using average drainage area pressure to evaluate the effectiveness of obtaining average drainage area pressure.

5.2.1. The Review of oscillation results on Unisim-I-D

The oscillations in rates of injection wells and production wells only appear in early and late production, shown in figure 5.17. The simulations in the previous chapter observed no oscillation because the initial time step is too big to observe early oscillation, and the total simulation time is too short to observe oscillation during late time production.

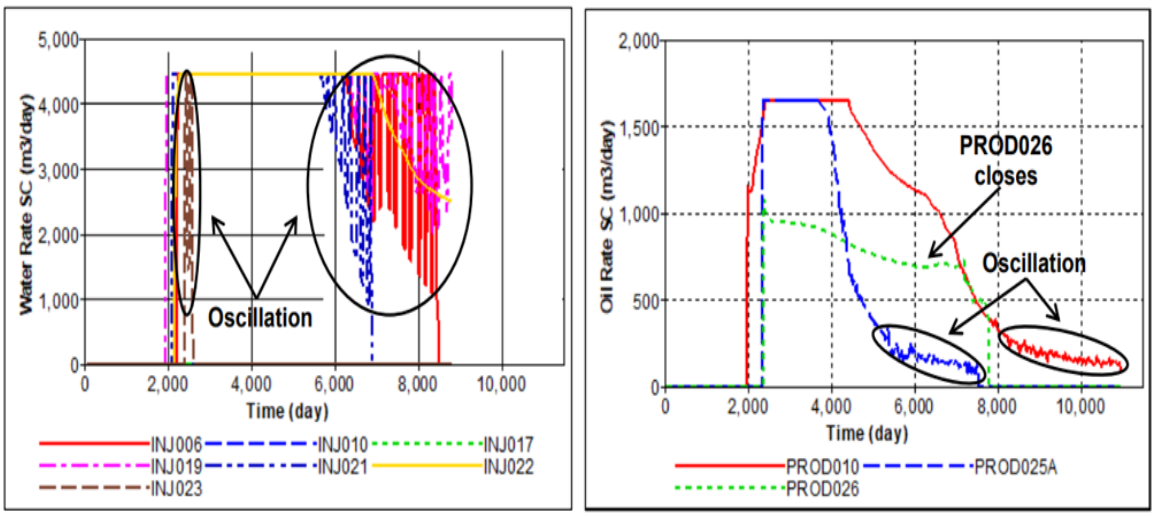

Figure 5.17 Rate of Wells – Explicit Coupling Without PID Controllers reprinted from (Gurjão, 2018).

5.2.2. Analysis with Simplistic Model

The simplistic reservoir is too large to observe late-time production in a short production period. However, reducing the size of the reservoir also reduces the size of the grid block. The size of the grid block could be a factor of error in well block pressure. A sensitivity analysis is performed on the size of the reservoir and the size of the grid block before evaluating the effectiveness of replacing block pressure by average drainage area pressure.

5.2.3. Sensitivity Analysis of the Size of Grid blocks and Reservoirs

Three simulations are run with the same grid block (25x25m size of grid block) but with different sizes of reservoirs to check the effectiveness of using drainage area pressure in different sizes of reservoirs. At the end of each time step, block pressure is compared with drainage area pressure to show the error in block pressure, shown in figure 5.18. Block pressure is less accurate in the smaller reservoir, and the percent error in the 1025x1025x30 meter reservoir is much larger than the error in the other two sizes of reservoirs.

The error of well block pressure is calculated with percent error, defined as

$$\text{Percent Error} = \left| \frac{P_{block} - \overline{P}}{\overline{P}} \right| \cdot 100\%. \tag{5.1}$$

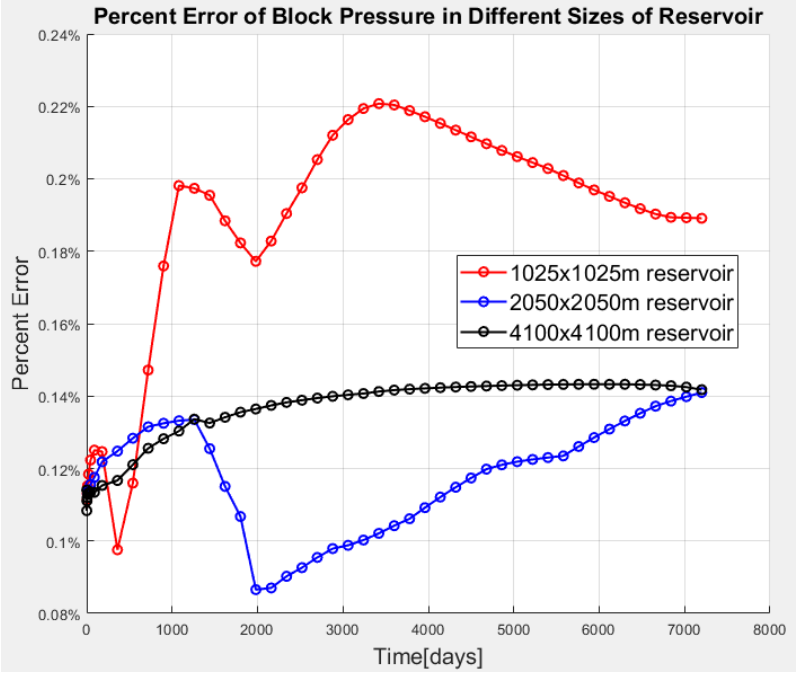

Figure 5.18 Sensitivity Analysis on Sizes of Reservoirs with 25x25m Grid Blocks.

Another three simulations are run with the same size of the reservoir (1025x1025x30m size of a reservoir) but with different sizes of the grid block to check the influence of different sizes of grid block on well block pressure. At the end of each time step, block pressure is compared with drainage area pressure to show the error in block pressure, shown in figure 5.19. Block pressure is less accurate for larger grid blocks. However, the difference in percent error is tiny, except for the very small size of a grid block. With a grid block size larger than 12.5x12.5m, the difference is error is negligible.

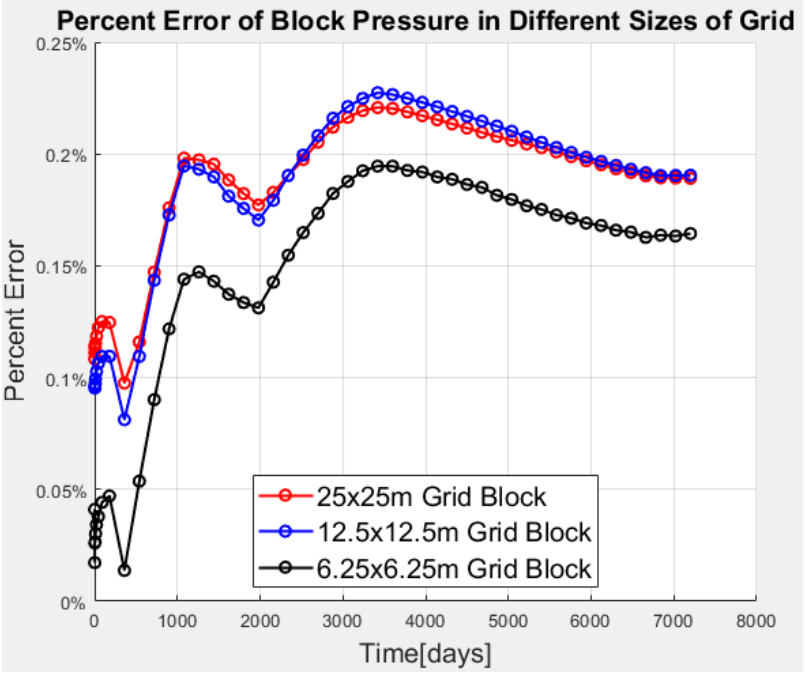

Figure 5.19 Sensitivity Analysis on Sizes of Grid blocks in 1025x1025x30m Reservoir.

5.2.4. Analysis of Oscillation

By further reducing the size of the reservoir, the late-time oscillation is observed in the 512x512x30m reservoir. The IPR is calculated from the drainage area pressure, but the oscillation still occurs. The percent error of block pressure is shown in figure 5.20.

For production wells, the error in well block pressure is minimal. The largest error does not exceed 0.25% before oscillation in the 512 meters by 512 meters reservoir, and even during oscillation, the error is very small. Therefore, inaccurate estimation of well block pressure is not the main reason for the oscillation for this case. The rate and pressure results are shown in figure 5.21 and figure 5.22. The late time oscillation is like behaviors in the transient flow but reversed, where the pressure distribution is not affected by the boundary. Also, pressure and pressure derivatives are a function of both time and position for transient flow, described by the following equation:

$$p(r,t) = p_i - \frac{q\mu}{4\pi kh} E_i\left(-\frac{\phi\mu c r^2}{4kt}\right). \tag{5.2}$$

And as a result, the productivity index is a function of time, which is the primary cause for oscillations in simulations with a large size of time steps.

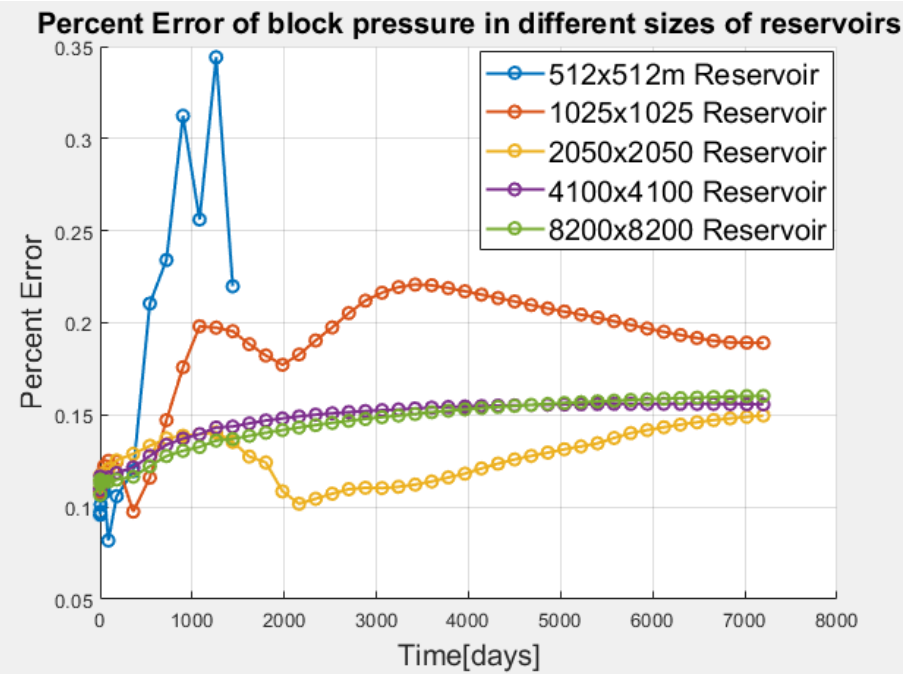

Figure 5.20 Percent Error of Well Pressure in The Simplistic Model.

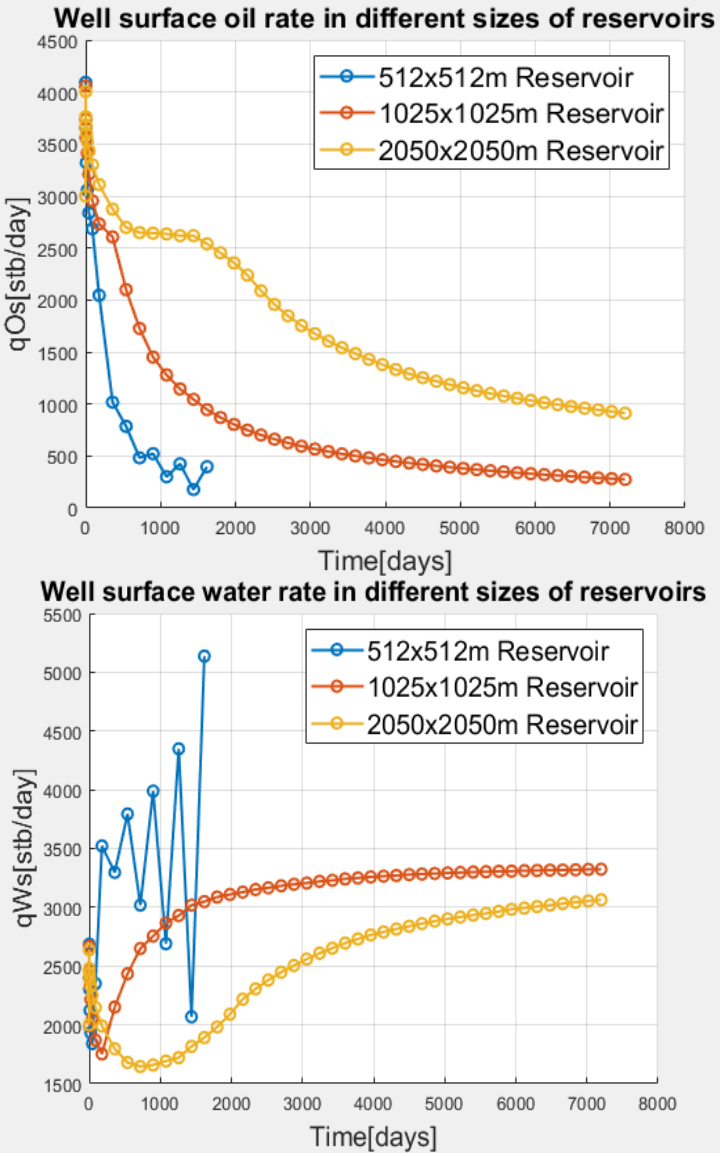

Figure 5.21 Surface Water and Oil Rate in Different Sizes of Reservoirs.

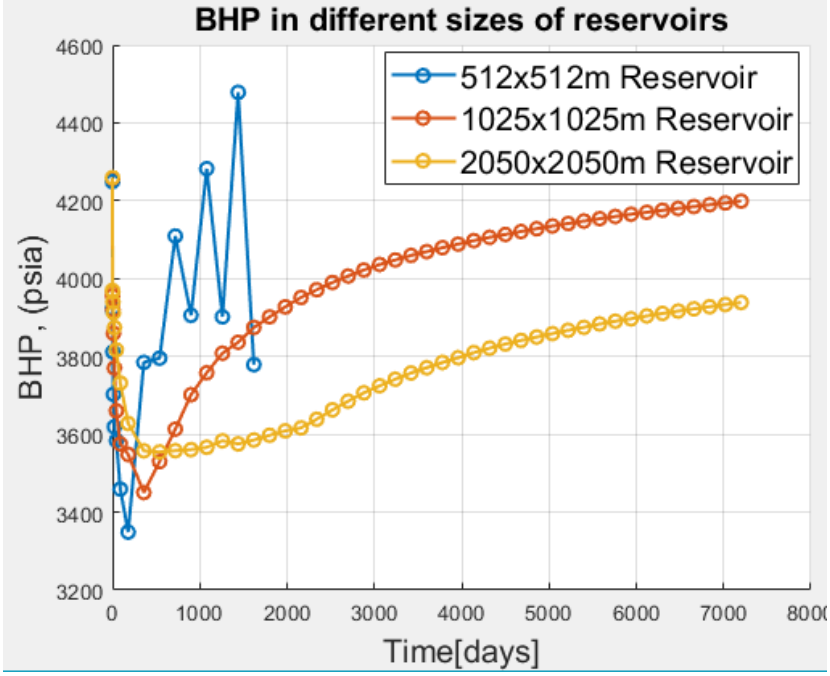

Figure 5.22 Bottom-hole Pressure in Different Sizes of Reservoirs.

For the injection well, figure 5.23 shows the oscillation in the water rate during the late time. Similarly, it's a result of having an injection index as a function of time for simulations with large time steps.

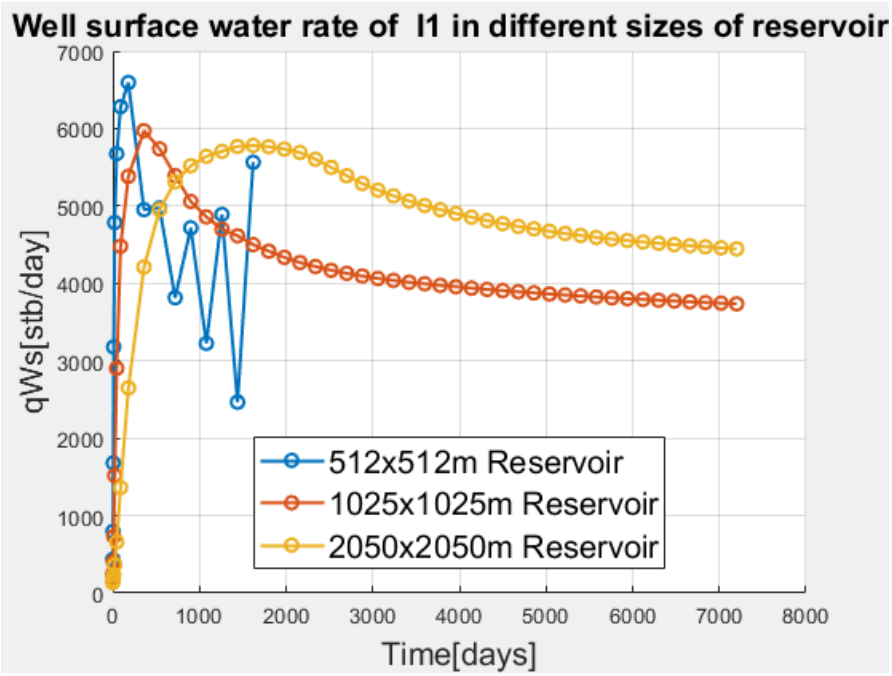

Figure 5.23 Surface Water Rate of I1 for Different Sizes of Reservoirs.

5.2.5. The Solution for Reducing Oscillation

When the size of the time step is large, the error in block pressure is not a significant problem, and the use of drainage area pressure for IPR calculation is less effective in reducing the oscillation. This oscillation is caused by having the reservoir pressure as a function of time. Therefore, to mitigate oscillation for large size of time steps, it's more reasonable to develop a method to reduce time step size. The advanced method that finds the optimum time step size using the PID controller is developed by Redick in 2017, is probably the best solution to this problem. However, a more straightforward solution is used in this study to show the effect of reducing the time step.

The oscillation also occurs in percent error of well block pressure, making it a good indicator to start reducing the time step. The indicator is defined using the percent change of the percent error as

$$\text{Percent change} = \frac{[\text{percent error}]_n - [\text{percent error}]_{n-1}}{[\text{percent error}]_{n-1}} \cdot 100\%, \quad \text{where } n \text{ is number of time step, and } n > 1. \tag{5.3}$$

Simulating the method of reducing the time step, we obtained stable results shown in figure 5.24. Besides, the water cut is very high at the beginning of the oscillation. Therefore, another method is to shut down wells above a certain value of water cut, for example, shutting above 90% of water cut.

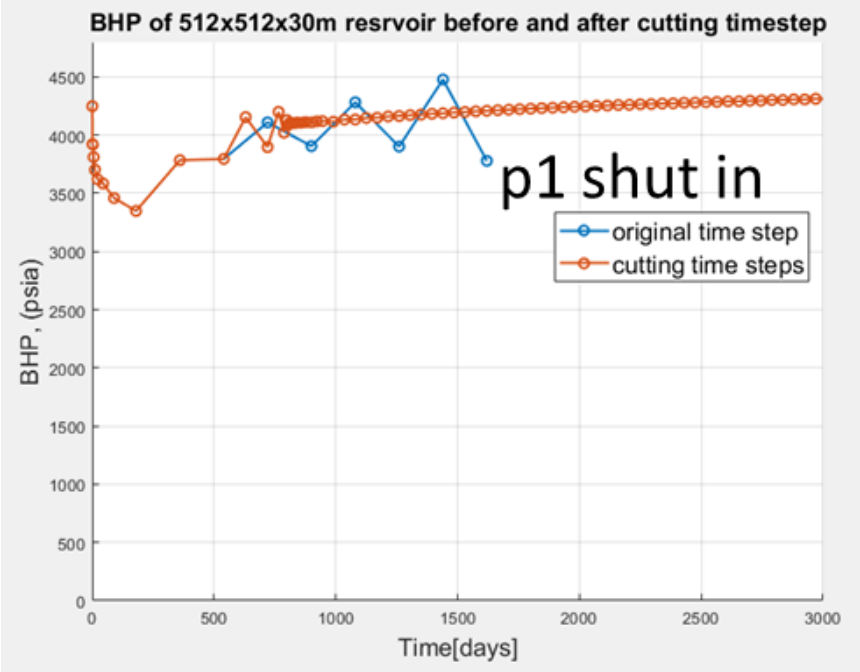

Figure 5.24 Reducing Oscillation by Cutting the size fo Time Steps.

5.2.6. Analysis of IPR Calculation with Surface Liquid Rate

In this study, all IPR calculations are using surface oil rates. However, for oscillations in late-time production, the water cut is so high that the water rate is much larger than the oil rate. The oscillation in the water rate is much larger than that of the oil rate as well. The percent error of Block pressure is plotted to compare the effectiveness of these two methods, shown in figure 5.25. By changing IPR calculations with surface oil rate to surface liquid rate, the error of block pressure increases during late-time production, so using the liquid rate for IPR calculation can obtain more accurate average drainage area pressure, shown in figure 5.26.

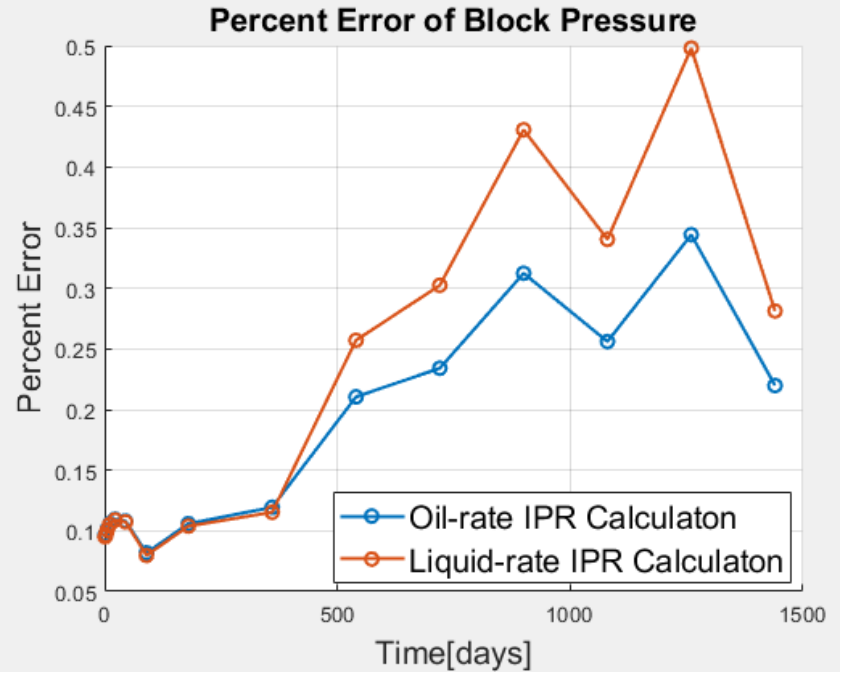

Figure 5.25 Percent Error of Different IPR Calculation methods.

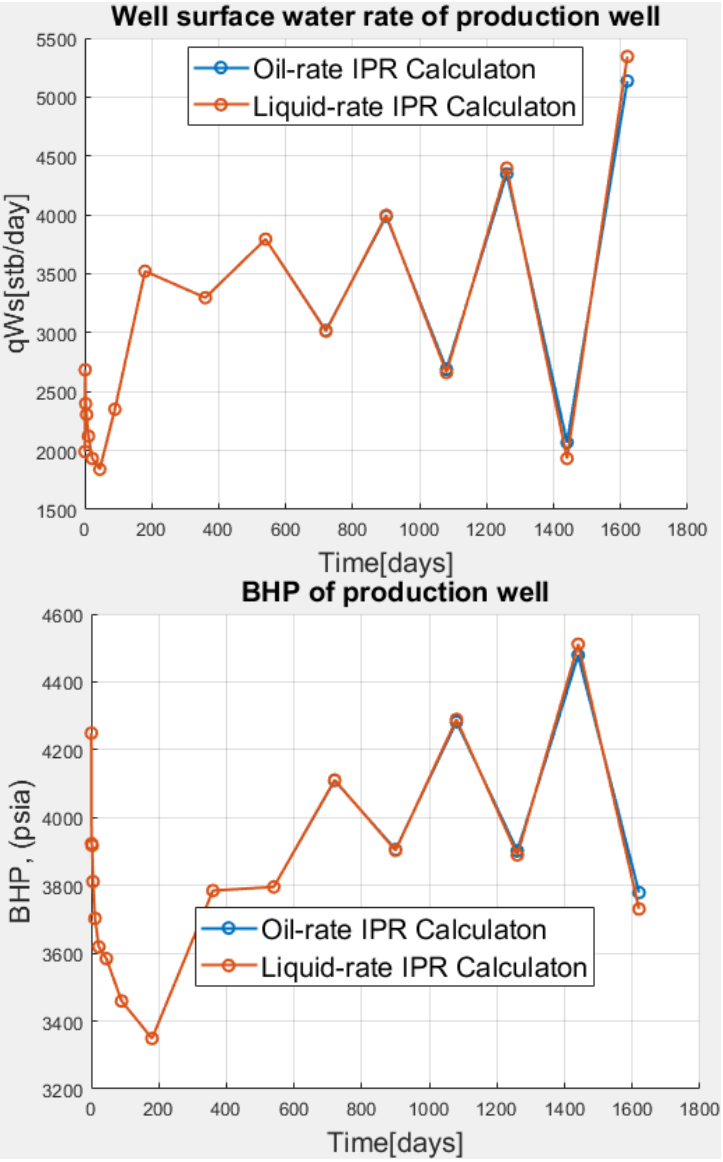

Figure 5.26 Surface Water Rate and BHP of Different IPR Calculation methods.

Although using the liquid-rate IPR calculation method results in more accurate average drainage area pressure, the oscillations in bottom-hole pressure and surface water rate are not reduced in this case. These results are expected because the previous section shows that the large size of time steps is a dominant factor of the oscillation and the solution to this oscillation is to reduce the size of time steps.

6. CONCLUSION

The surface network coupling is illustrated in two types of models. The surface coupling module can perform stable explicit coupling for production and injection well during pseudo-steady state and steady-state flow. The computational cost of obtaining average area pressure is reasonable but could be expensive for a smaller size of time steps.

Using average drainage area pressure for IPR calculation can improve accuracy and possibly reduce oscillation for small-sized steps. However, this will not mitigate oscillations in simulations with a large size of time steps in the late-time production.

The error of well block pressure is low in smaller grids, and therefore block pressure is a good representation of the drainage area when using smaller grids. However, solving simulations with smaller grid blocks could exponentially increase the computational cost.

During late-time production, where surface water rate is the primary producing fluid, using the surface liquid rate for IPR calculation can obtain more accurate average drainage area pressure than using the surface oil rate for IPR calculation.

The oscillation for simulation with a large size of time steps is mainly caused by a reversed transient flow behavior, where pressure and productivity index is a function of time. Therefore, it's more reasonable to solve the oscillation problem by reducing the size of time steps. The best available method is using the PID controller to optimize the time step size developed by Redick in 2017.

6.1. Future work

With the developed toolbox for production-reservoir system coupling in MRST, future work could be the following:

- Development of other basic surface components, such as manifold which is a more complex component.
- Application of explicit coupling for gas or volatile oil fields, by adding other fluid properties for different types of fluid.
- Development of methods to design and optimize the surface network for the large offshore field.
- Development of methods to determine optimum production strategy for oil and gas fields.

REFERENCES

Avansi, G. D., Schiozer, D. J., 2015, *UNISIM-I: Synthetic Model for Reservoir Development and Management Applications. International Journal of Modeling and Simulation for the Petroleum Industry*, v. 9, n. 1, pp. 21-30

Beggs, H. D.; Brill, J. P., 1973, A Study of Two-Phase Flow in Inclined Pipes. *Journal of Petroleum Technology*. *AIME*. 255 (SPE-4007-PA).

Beggs, H. D.; Brill, J. P., 1991, *Two Phase Flow in Pipes*, University of Tulsa, Tulsa, Oklahoma

Brown, Kermit, 1984, *The Technology of Artificial Lift Methods. Volume 4. Production Optimization of Oil and Gas Wells by Nodal System Analysis*. Tulsa, Oklahoma: PennWellBookss

Dake, L P., 1978, *Fundamentals of Reservoir Engineering*. Amsterdam: Elsevier Scientific Pub. Co,. Print.

DeBaun, D., Byer, T., Childs, P., Chen, J., Saaf, F., Wells, M., Liu, J., Cao, H., Pianelo, L., Tilakraj, V., Crumpton, P., Walsh, D., Yardumian, H., Zorzynski, R., Lim, K.-T., Schrader, M., Zapata, V., Nolen, J., and Tchelepi, H. A, 2005, An extensible architecture for next generation scalable parallel reservoir simulation. In SPE Reservoir Simulation Symposium, 31 January–2 Feburary, The Woodlands, Texas, USA.

Economides, M.J., Hill, A.D., Ehlig-Economides, C. and Zhu, D., 2013, *Petroleum Production Systems*, Upper Saddle River: Prentice Hall.

Ertekin, Turgay, J. H. Abou-Kassem, and G. R. King., 2000, *Basic Applied Reservoir Simulation*. Richardson, US: Society of Petroleum Engineers. Web.

Gurjão, K. G. R., 2018, Oscillation Mitigation in Subsurface and Surface Couplings Using PID Controllers. MSc thesis. Campinas: University of Campinas (Unicamp).

Guyaguler, B., Zapata, V. J., Cao, H., Stamati, H. F., & Holmes, J. A., 2011, Near-Well-Subdomain Simulations for Accurate Inflow-Performance-Relationship Calculation To Improve Stability of Reservoir/Network Coupling. Society of Petroleum Engineers. doi:10.2118/141207-PA

Hayder, E. M., Dahan, M., & Dossary, M. N., 2006, Production Optimization through Coupled Facility-Reservoir Simulation. Society of Petroleum Engineers. doi:10.2118/100027-MS

Hiebert, A. D., Khoshkbarchi, M., Sammon, P. H., Alves, I. N., Rodrigues, J., Belien, A. J., … Valvatne, P., 2011, An Advanced Framework for Simulating Connected Reservoirs, Wells and Production Facilities. Society of Petroleum Engineers. doi:10.2118/141012-MS

Hohendorff Filho, J. C. V., Schiozer, D. J. A Correction Methodology for Explicit Coupling between Reservoir and Production System Simulators. *XXXVII Iberian Latin American Congress on Computational Methods in Engineering*, Brasilia, Brazil, November 2016.

Jansen, J. D., 2017, *Nodal Analysis of Oil and Gas Production Systems*. Richardson: SPE.

K.-A. Lie, S. Krogstad, I. S. Ligaarden, J. R. Natvig, H. M. Nilsen, and B. Skaflestad., 2012, Open source MATLAB implementation of consistent discretisations on complex grids. *Computational Geosciences*, Vol. 16, No. 2, pp. 297-322.

Liang, J., & Rubin, B., 2013, A Semi-Implicit Approach for Integrated Reservoir and Surface Network Simulation. Society of Petroleum Engineers. doi:10.2118/163615-MS

Lie, Knut-Andreas., 2019, *An Introduction to Reservoir Simulation Using MATLAB/GNU Octave: User Guide for the MATLAB Reservoir Simulation Toolbox (MRST)*. Cambridge University Press.

Peaceman, D. W., 1978, Interpretation of Well Block Pressure in Numerical Reservoir Simulation. *SPE Journal* (SPE 6893), v. 18, n. 3.

Redick, B. S., 2017, PID Controlled Adaptive Time Stepping in Coupled Surface-Subsurface Simulation: A Tool for Reducing Non-Physical Oscillation. MSc thesis. College Station: Texas A&M University.

Rivaie, Mohd & Fakhri, Muhammad & Hayati, Nujma & Ramli, Nurul & Jusoh, Ibrahim., 2017, The n-th section method: A modification of Bisection. *Malaysian Journal of Fundamental and Applied Sciences*.

S. Krogstad, K.-A. Lie, O. Møyner, H. M. Nilsen, X. Raynaud, and B. Skaflestad., 2015, *MRST-AD - an open-source framework for rapid prototyping and evaluation of reservoir simulation problems*. 2015 Reservoir Simulation Symposium, Houston, Texas, USA, 23-25 February 2015.

Van Everdingen, A. F., 1953, The Skin Effect and Its Influence on the Productive Capacity of a Well. *Journal of Petroleum Technology*. doi:10.2118/203-G

Zhang, Y., Seth, G. Chen, J., 2017, A Novel IPR Calculation Technique to Reduce Oscillations in Time-Lagged Network-Reservoir Coupled Modeling Using Analytical Scaling and Fast Marching Method. SPE 182704. SPE Reservoir Simulation Conference, Montgomery, Texas, USA, February 2017.

APPENDIX A

MODIFIED FILES IN MRST

In the latest MRST version, 2020a, two error in programing was found in two files. An error is found in expandPVCOintoPVTO.m, which reads the PVCO table. The columns are read in the wrong order and should be fixed with the order shown in figure A.1. This file is located in the following path:

mrst-2020a\modules\deckformat\deckinput\private\expandPVCOintoPVTO.m

```
27      for i = 1:ntab
28          tloc = tbl{i};
29
30          %wrong columns; modified by Zihao Chen Sep 6th 2020
31          tloc = tloc(:,[2 1 3 4 5 6]);
32
```

Figure A.1 Modification of expandPVCOintoPVTO.m in MRST 2020a.

Another error is found in getMinMaxPhaseSaturations.m, which initializes saturation for the reservoir. Water saturation was initialized differently from the initialization of Eclipse, where connate water saturation was used for minimum saturation. The modification of this file is shown in figure A.2. This file is located in the following path:

mrst-2020a\modules\ad-core\initialization\getMinMaxPhaseSaturations.m

```
101         else
102             s_max(:, i) = pts.(ph)(subs, max_sub);
103     %       s_min(:, i) = pts.(ph)(subs, min_sub);
104     %%      modified by Zihao Chen Sep. 2nd 2020
105             if strcmp(ph, 'w')
106                 s_min(:, i) = pts.(ph)(subs, min_sub-1);
107             else
108                 s_min(:, i) = pts.(ph)(subs, min_sub);
109             end
```

Figure A.2 Modification of getMinMaxPhaseSaturations.m in MRST 2020a.

APPENDIX B

THE SETTING OF THE DEVELOPED MODULES

The setting of the surface network is stored in two new structures introduced in section 4.4, in figure 4.7 and 4.8. The construction of these structures is using two functions shown in figure B.1.

```
%% Set Surface network system
networks = SurfaceNetwork_UNISIM(schedules);
nwsystem = getnetworksystem(model,schedules,networks, 'useMex',true, ...
                                                       'PVTO',true);
```

Figure B.1 Functions for the setting of the surface network.

The SurfaceNetwork_UNISIM function is used to set the surface network setting for each well. The input parts of this function for different cases are shown in the network settings sections in figure B.2.

```
    %% network settings
    Length_Riser = 166*meter  * ones(1,NumberofProdWell);
    Length_flowline = [1045,2600,1325,1845,2750,3456,1789,1125,1298, ...
                                          2025,1425, 1193,1074,1544];
    Length_Tubing = [W.refDepth]-Length_Riser;

    for n = 1:NumberofProdWell
        %% network settings
        ncs = 3;
        network = initializenetwork(ncs);
        %% input
        comp_name = {'Separator';'Riser';'Flowline';'Tubing'};
        comp_type = {[];1;1;1};
        comp_model = {[];1;1;1};
        comp_diameter = {[];6*inch;6*inch;4.5*inch};
        comp_inclination = {[];0;90*degree;0};
        comp_roughness = {[];30e-6;30e-6;30e-6};
        comp_length = {[];Length_Riser(n);Length_flowline(n);Length_Tubing(n)};
        comp_T_bottom = {20;40;70;80};
        comp_Psep = {100*psia;[];[];[]};

        %% assign setting
        input = {comp_name;comp_type;comp_model;comp_diameter; ...
                 comp_inclination;comp_roughness;comp_length;  ...
```

Figure B.2 The Input Sections in SurfaceNetwork_UNISIM.

The getnetworksystem function is used to assemble the surface network settings with other parameters, such as the type of correlations using for modeling and the bottom-hole temperature. The input parts of this function for different cases are shown in the inputs sections in figure B.3.

```
    %initialize
    W = schedules.control.W;
    W = W([W.sign] == -1);
    NumberofProdWell = length(W);
    nwsystem = cell2struct(cell(1,NumberofProdWell), 'Wellname');

%--------------------------------------------------------------------------
    %inputs
    Blackoilcorrelation = num2cell( 1  * ones(1,NumberofProdWell)); % 1 =Standing; 2 =Glaso
    Temp_Bottomhole     = num2cell( 80 * ones(1,NumberofProdWell)); %celsius
    Reservoir_Region    = num2cell( 1  * ones(1,NumberofProdWell));

%--------------------------------------------------------------------------
    %assigning values
    [nwsystem.Wellname] = W.name;
```

Figure B.3 The Input Sections in SurfaceNetwork_UNISIM.

The Surface_coupling function is used to couple the reservoir and production system. Different solver could be used for solving the reservoir simulation and for solving an additional point for IPR calculation, shown in figure B.4. The 'usePblock' option could be changed to true to construct the IPR curve with block pressure. The 'oldresults' option could be used for continued simulation by changing the empty brackets with the output structure of the Surface_coupling function.

```
%% Surface coupling
nls = getNonLinearSolver(model,'useCPR',true);
nlsl = getNonLinearSolver(model,'useCPR',false);
Results = Surface_coupling(initState, model, schedules, nwsystem, ...
                                                    'usePblock',false, ...
                                                'nonlinearsolver',nls, ...
                                                     'IPRsolver',nlsl, ...
                                                     'oldresults',[]);
```

Figure B.4 The setting of Surface_coupling function.

The Surface_coupling function assembles the IPR calculation methods, the IPRfunc function,and coupling methods, the coupling function, shown in figure B.5. These functions could be altered for the development of new techniques.

```
%IPRfun for producers and injector
tic
[IPRfun,Wn,Optinj,INJIPR] = IPRfunc(Wellsol,ST,schedule,  ...
                                          model,nwsystem,  ...
                                    'usePblock',opt.usePblock,...
                                    'nonlinearsolver',IPRnls);
Elapsedtime(n,2) = toc;

% coupling producers
tic
[Optprod,OPRout] = coupling(IPRfun,Wn,Wellsol,nwsystem,'maxiteration', 50,...
                                               'Tol', 1e-6, 'npt',4);
```

Figure B.5 Main Functions in the Surface_coupling function.